©2016 Society of Economic Geologists, Inc.
Economic Geology, v. 111, pp. 1439–1463

Ambient Redox and Hydrothermal Environment of the Wolverine Volcanogenic Massive Sulfide Deposit, Yukon: Insights from Lithofacies and Lithogeochemistry of Mississippian Host Shales*

Stephen J. Piercey,[1,†] Harold L. Gibson,[2] Nicole Tardif,[2,**] and Balz S. Kamber[3]

[1] *Department of Earth Sciences, Memorial University, St. John's, Newfoundland, Canada A1B 3X5*

[2] *Mineral Exploration Research Centre, Department of Earth Sciences, Laurentian University, Sudbury, Ontario, Canada PE3 6L3*

[3] *Department of Geology, Trinity College Dublin, Dublin 2, Ireland*

Abstract

The Wolverine volcanogenic massive sulfide (VMS) deposit is a polymetallic, felsic-siliciclastic deposit hosted by ~352 to 347 Ma volcanic and sedimentary rocks of the Yukon-Tanana terrane, Yukon, Canada. Shales are located at various stratigraphic levels and in various mineralized zones within the Wolverine deposit area (e.g., Fisher, Puck, and Sable zones). Shales present along the mineralized horizon near the immediate hanging wall and footwall were deposited under anoxic conditions (e.g., low Mn, anoxic V-Cr-Mo-U systematics), whereas in the stratigraphically deeper footwall and uppermost hanging wall, the redox signatures imply deposition under suboxic to oxic conditions. The Mo-U systematics of the shales suggest that during the time of sulfide mineralization, the ambient basin was periodically euxinic with aqueous H_2S present in the water column that this H_2S contributed to the sulfur budget of the deposit. Furthermore, the Mo-U and C_{org}-Ni systematics favor deposition in a restricted basin (i.e., nutrient trap) where restriction of the water column led to H_2S formation via sulfate reduction associated with excess organic carbon preservation. There is also evidence of a progressive shift upward in the stratigraphy to more oxygenated conditions in the uppermost hanging wall. The shift from euxinic to oxic-suboxic conditions is consistent with regional tectonic models that indicate a change from rifting during Wolverine deposit formation, where the basin was partially restricted with minimal circulation (i.e., restricted depocenter), to an incipient back-arc basin accompanied by extension and likely ingress of oxygenated seawater.

The rare earth element and Y (REY) systematics in Wolverine shales illustrate that proximal to the mineralized horizon, shales have higher Y/Ho (>27), and Ce/Ce*<<1 and negative Ce anomalies indicative of oxygenated seawater. The Ce/Ce* values in the Wolverine shales have an inverse correlation with P_2O_5 content and suggest partial control by detrital apatite. It is envisioned that apatite formed in the upper, oxygenated portion of the water column, inherited the REE signature of oxygenated seawater (i.e., Ce/Ce*<<1), and was subsequently deposited into deeper waters as detrital grains. The Ce/Ce* and Y/Ho also correlate with CO_2 and carbonate content of the shales. Moreover, the shales that have the strongest REY signature of oxygenated seawater also coincide with the strongest euxinic signatures. This paradox can be reconciled by enhanced deposition of apatite coincident with deposit formation, coupled with a late hydrothermal overprint on the shales from low-temperature, CO_2-rich (oxygenated?) hydrothermal fluids (i.e., high Y/Ho and Ce/Ce*<<1) in a vent-proximal environment. This model is consistent with the geology, stratigraphy, and hydrothermal alteration in the immediate footwall and hanging wall of the deposit.

Prospective shales in the Wolverine basin, and similar sediment-rich hydrothermal basins globally, should exhibit evidence for deposition under anoxic conditions (i.e., Mn <1,000 ppm; high V-Mo-U, U_{EF}, Mo_{EF}), hydrothermal Fe-Al-Mn systematics (i.e., high Fe/Al), and evidence for hydrothermal alteration (i.e., high CIW values, high molar sericite and chlorite). Identification of samples having these features is useful in targeting prospective VMS environments in shale-dominated successions and potential targets within shale-rich basins.

Introduction

The Wolverine volcanogenic massive sulfide (VMS) deposit represents a type example of a shale-rich VMS deposit (Bradshaw et al., 2008). The deposit is located within the Finlayson Lake VMS district, Yukon (Fig. 1), and is hosted by Early Mississippian (~352–347 Ma) rocks of the Yukon-Tanana terrane (Murphy et al., 2006). The Wolverine deposit has numerous features traditional to VMS deposits, including volcanic host rocks, metal zoning patterns, and typical sericite and chlorite alteration of footwall strata (e.g., Franklin et al., 2005; Galley et al., 2007; Bradshaw et al., 2008). However, the deposit is unlike classic mound-like VMS deposits in containing mineralization that is tabular in nature, has abundant shale in the host stratigraphy, and sulfides with both very light (biogenic) and very heavy $\delta^{34}S$ values, similar to those of sedimentary-exhalative mineralization (e.g., Bradshaw et al., 2008). The latter characteristics of Wolverine are similar to other felsic siliciclastic VMS deposits in shale-rich environments, such as those in the Bathurst mining camp (e.g., Brunswick 12) and the Iberian pyrite belt (Neves Corvo, Tharsis), for which workers have suggested mineralization formed via the venting of VMS-related hydrothermal fluids into an anoxic basin, similar to the ambient environment in which SEDEX deposits form (Goodfellow and Peter, 1996; Goodfellow et al., 2003b; Tornos et al., 2008; Menor-Salvan et al., 2010; Sáez et al., 2011).

At the Wolverine deposit an intimate spatial relationship exists between shales and sulfide mineralization, with shales

† Corresponding author: e-mail, spiercey@mun.ca

* A digital Appendix to this paper is available at http://economicgeology.org/ and at http://econgeol.geoscienceworld.org/.

** Present address: Goodman School of Mines, Laurentian University, 935 Ramsey Lake Rd., Sudbury, Ontario, Canada P3E 2C6.

Submitted: November 24, 2014
Accepted: May 4, 2016

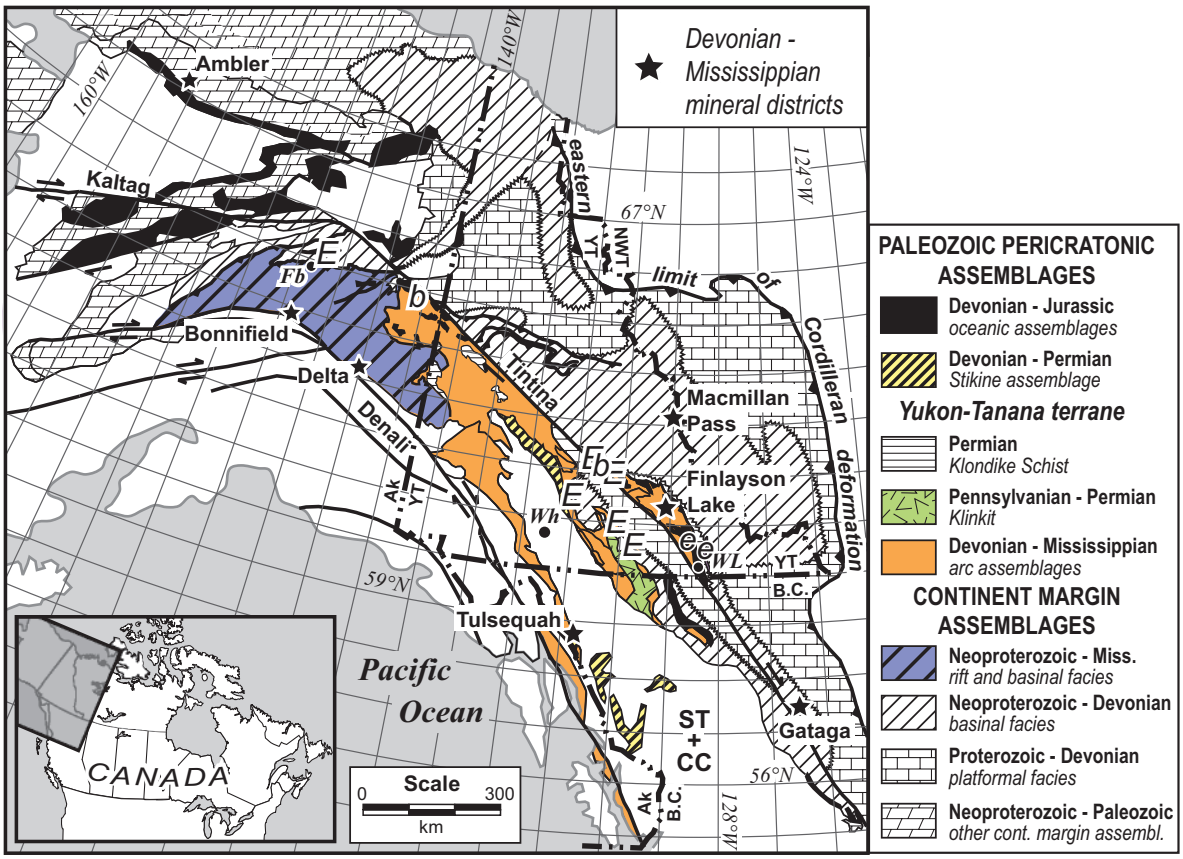

Fig. 1. Terrane map of northern Cordillera, showing location of Finlayson Lake district. Stars on the map are VMS or sediment-hosted Zn-Pb districts. Modified from Colpron et al. (2006). Abbreviations: (locations) Fb = Fairbanks, ST + CC = Stikine and Cache Creek Terranes, Wh = Whitehorse, WL = Watson Lake; (rocks) b = blueschist, e = eclogite (Mississippian), E = eclogite (Permian).

occurring in the immediate hanging wall to mineralization, stratigraphically below (i.e., within 10s to 100s m), and hundreds of meters above mineralization. Furthermore, numerous prospects occur along strike (e.g., Fisher, Puck, Sable) that also contain shales with and without mineralization. The Wolverine deposit thus presents an opportunity to understand changes in the chemistry of shales as a function of stratigraphic position, and of proximity and distance from mineralization. Previous work on shale geochemistry and mineralogy, in general, and specifically in other felsic siliciclastic VMS deposits, has provided critical information on the relationship of shales to mineralization, including information on the provenance of the sediments, the importance of hydrothermal activity, and the ambient ocean redox environment during deposit formation (Raiswell and Berner, 1985; Calvert and Pedersen, 1993; Quinby-Hunt and Wilde, 1994, 1996; Goodfellow et al., 2003b; Meyer and Kump, 2008; Piper and Calvert, 2009; Sáez et al., 2011).

In this paper we provide a detailed geologic and lithogeochemical study of shales from the Wolverine VMS deposit. Goals of the paper are to (1) evaluate the setting of shales and their relationship to mineralization, (2) use bulk geochemistry of the shales to constrain the ambient redox environment during deposit formation, and (3) use the shales to understand their role in localizing mineralization and their potential as a exploration vector for VMS mineralization in shale-rich basins.

Regional Geology

The Finlayson Lake district consists of rocks from the Yukon-Tanana and Slide Mountain terranes northeast of the Tintina fault, in southeastern Yukon (Fig. 1). These terranes represent a continental arc and back-arc basin sequence that developed along the ancient Pacific margin of North America, in the middle to late Paleozoic (Late Devonian through Permian), similar to the present-day tectonic configuration of Japan, the Japan Sea, and the Sino-Korean craton (Nelson et al., 2006; Piercey et al., 2006). The district consists of pericratonic rocks of the Yukon-Tanana terrane and oceanic rocks of the Slide Mountain terrane that are juxtaposed against rocks of the North American continental margin along the Inconnu thrust of post-Late Triassic age (Figs. 2, 3; Murphy et al., 2006). The Yukon-Tanana and Slide Mountain terranes in the Finlayson Lake district contain variably deformed and metamorphosed, lower greenschist- to amphibolite-facies metasedimentary and metavolcanic rocks and affiliated metaplutonic suites. Rocks of the terrane are foliated and variably folded; however, primary features and geochemical characteristics are locally well preserved (e.g., Murphy et al., 2006; Piercey et al., 2006).

The Finlayson Lake district is subdivided into several informal fault- and unconformity-bounded groups and formations (Figs. 2, 3; Murphy et al., 2006). The structurally deepest units of the Yukon-Tanana terrane occur in the footwall of the Money Creek thrust, an Early Permian east-northeast-vergent thrust fault having more than 35 km of displacement that juxtaposes broadly coeval, but lithologically and geochemically distinct, lithologic successions. Rocks in the footwall of the thrust include mafic and felsic metavolcanic and metasedimentary rocks of the Upper Devonian and older Grass Lakes Group, Late Devonian to Early Mississippian metagranitic rocks of the Grass Lakes plutonic suite, and metasedimentary and mafic and felsic metavolcanic rocks of the unconformably overlying Lower Mississippian Wolverine Lake Group (Figs. 2, 3). The Grass Lakes Group is host to the Fyre Lake, Kudz Ze Kayah, and GP4F VMS deposits, whereas the Wolverine Lake Group hosts the Wolverine deposit. The Grass Lakes and Wolverine Lake Groups have been interpreted to represent a continental back-arc rift to back-arc basin assemblage (Piercey et al., 2001a, b, 2004, 2006; Murphy et al., 2006).

The hanging wall of the Money Creek thrust consists of Upper Devonian to Lower Mississippian metasedimentary and felsic to intermediate metavolcanic rocks and granitoids (Mortensen, 1992), Lower Permian limestone, and, locally, Lower Permian dark-gray basinal clastic rocks (Figs. 2, 3). These latter rocks are overlain by an upper thrust package, which comprises undeformed, predominantly Late Devonian mafic volcanic rocks of the Cleaver Lake Formation, spatially associated and probably comagmatic felsic, mafic, and ultramafic metaplutonic rocks, and a crosscutting Early Mississippian pluton of the Simpson Range plutonic suite. None of these rock units hosts significant VMS mineralization. The rocks of the hanging wall of the Money Creek thrust (Cleaver Lake Formation and Simpson Range plutonic suite) have been interpreted to represent the products of continental-arc magmatism (Grant, 1997; Piercey et al., 2001b, 2003, 2006; Murphy et al., 2006).

To the north and east, imbricated rocks of the Yukon-Tanana terrane are juxtaposed against rocks of the Slide Mountain terrane along the Jules Creek fault (Figs. 2, 3). In this area, the Slide Mountain terrane comprises Mississippian to Lower Permian metasedimentary and metavolcanic rocks of the Fortin Creek Group. The Slide Mountain terrane also contains pristine to weakly foliated Lower Permian basalt, mafic and ultramafic plutonic rocks, and minor sedimentary rocks of the Campbell Range Formation. Mafic rocks of the Slide Mountain terrane are host to the Ice VMS deposit (Figs. 2, 3) and are interpreted to have formed in a Permian back-arc basin (Plint and Gordon, 1997; Piercey et al., 2006, 2012).

Wolverine Deposit Stratigraphy and Shale Relationships

The Wolverine deposit contains a distinctive lithostratigraphy in the footwall and hanging wall in which shales occur at different stratigraphic levels interlayered with volcano-sedimentary rocks (Figs. 4–7). The deepest part of the footwall consists predominantly of shale interbedded with fine-grained, variably quartz- and feldspar-bearing rhyolitic tuffs (Figs. 4–7; Bradshaw, 2003; Bradshaw et al., 2008). The immediate footwall is quartz-feldspar tuff with lesser shale. The footwall rocks are intruded by two generations of porphyritic rhyolitic sills, including an older suite of quartz-feldspar porphyritic rhyolite (~352 Ma), and a younger suite of feldspar porphyritic rhyolite (~347 Ma); both suites are spatially associated with mineralization and occur within tens of meters of mineralization in the Wolverine/Lynx zones (Fig. 5; Piercey et al., 2008). The hanging wall of the Wolverine deposit has been previously interpreted to be aphyric rhyolite intercalated with shale, carbonate exhalite, iron formation, silica-pyrite exhalite, and rhyolite breccia, and all capped by basalt (Figs. 4, 5; Bradshaw et al., 2008). However, mapping of lithofacies and alteration by Piercey and Gibson (unpub.) and Piercey et al. (2006) have revised stratigraphic units in the hanging wall, with the result that most rocks previously considered aphyric rhyolite are included within a laminated, crystal-poor rhyolitic siltstone that is variably interlayered with carbonaceous shale (Fig. 6). The rhyolitic siltstone is attributed to deposition from volcanic-ash-rich turbidity currents (Piercey and Gibson, 2005; Piercey et al., 2006). The rhyolite breccias above the uppermost iron formation contain fragments that are identical to the underlying rhyolite siltstone/tuff, and are thus interpreted to be reworked rhyolitic siltstone (Figs. 4, 5; Piercey and Gibson, 2005; Piercey et al., 2006). All other lithofacies are similar to those outlined by Bradshaw et al. (2008).

Massive sulfide mineralization at the Wolverine deposit occurs in three main zones: Wolverine and Lynx that are geographically separated by the Hump zone (Fig. 8). The Wolverine and Lynx zones are superficially similar in containing abundant Zn- and Pb-rich massive sulfide near upper contacts with Cu content increasing at depth and into the footwall (Bradshaw et al., 2008). The immediate footwall to mineralization in both zones is a crystal-rich rhyolitic tuff that contains variable amounts of carbonaceous material, commonly as interlayers or drapes on more rhyolitic tuffaceous layers (Figs. 4–7, 9). The footwall shows a distinctive lateral and vertical zonation in alteration from intense chlorite proximal to Cu-rich stringer and disseminated mineralization and more sericite at depth and distal from mineralization (Bradshaw et al., 2008). Volcaniclastic rocks are abundant in the footwall and proximal to massive sulfide mineralization, as are carbonaceous argillites/shales (Figs. 4-6, 9). The immediate hanging wall consists of either carbonaceous shale or carbonate-exhalite and these are conformably overlain, in turn, by carbonaceous shale interlayered with rhyolitic siltstone and iron formation, rhyolite siltstone breccias, and upper carbonaceous shale, all being capped by basalt, mafic volcaniclastic rocks, and graywacke (Figs. 4–7, 9; Bradshaw, 2003; Piercey and Gibson, 2005; Piercey et al., 2006; Peter et al., 2007; Bradshaw et al., 2008). The hanging-wall alteration of felsic volcanic and volcaniclastic rocks is widespread and extends upward to the upper iron formation, consisting predominantly of quartz with lesser sericite; in immediate proximity to mineralization and the carbonate exhalites is intense Fe carbonate alteration.

Along strike, other mineralized zones at Wolverine occur at a similar stratigraphic level as the main Wolverine deposit, but contain only minor sulfides (Figs. 4, 7). The hanging wall and footwall strata to the Fisher zone are similar to those of the Wolverine deposit, including in the footwall minor intervals of sericite- to chlorite-altered, felsic tuff with narrow bands of sphalerite-pyrite-galena and a thick sequence of fold-repeated

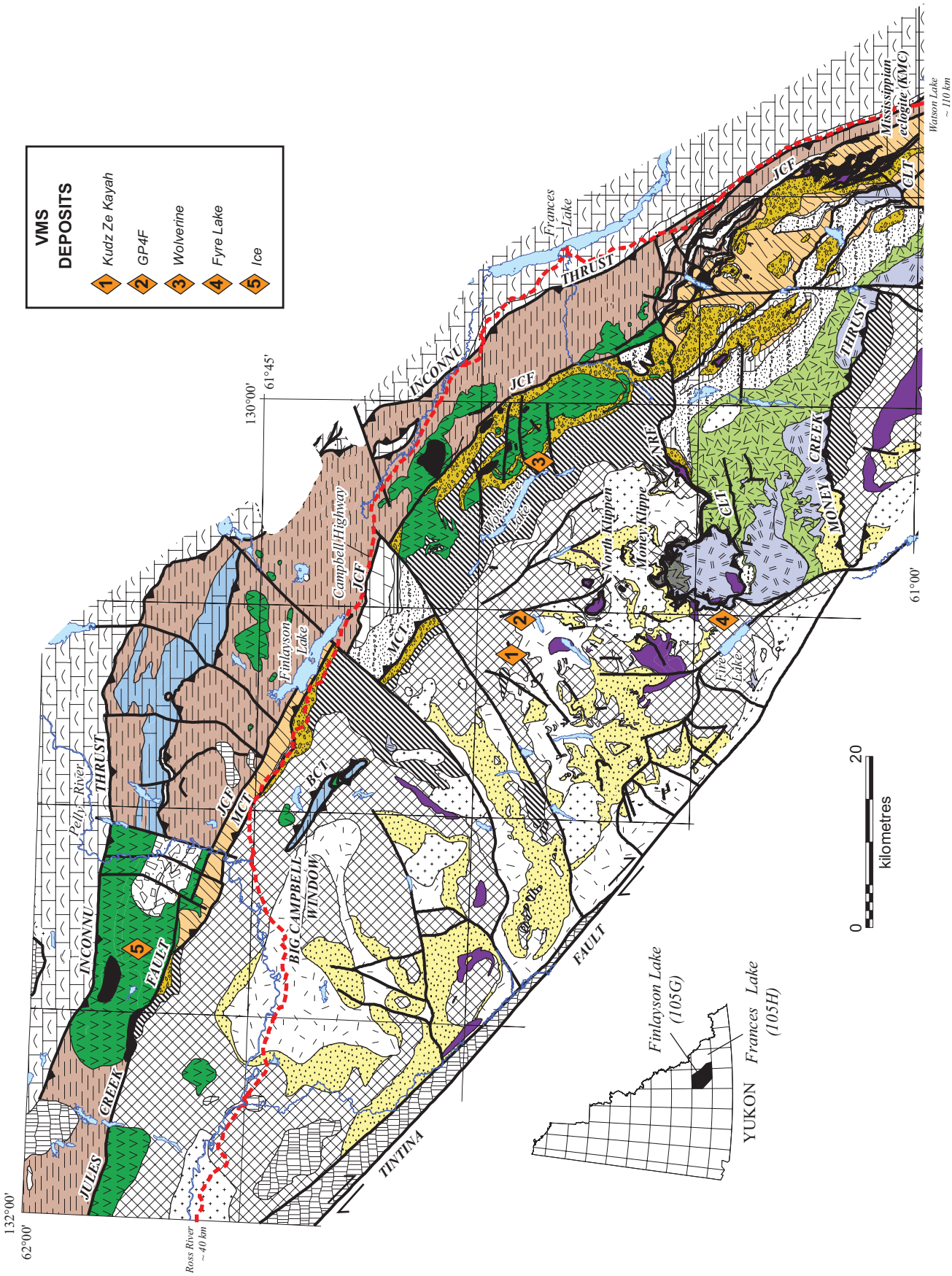

Fig. 2. Geologic map of Finlayson Lake district, showing locations of volcanogenic massive sulfide deposits (from Murphy et al., 2006). Abbreviations: BCT = Big Campbell Thrust, CLT = Cleaver Lake thrust, MCT = Money Creek thrust, NRF = North River Formation, SMT = Slide Mountain terrane.

LEGEND

Mesozoic and Cenozoic

undifferentiated intrusions

undifferentiated volcanic rocks

NORTH AMERICAN CONTINENTAL MARGIN

Triassic

dark shale, siltstone and limestone

Paleozoic

undifferentiated formations of Selwyn Basin, McEvoy Platform, Earn Group and Mt. Christie Formation

POST - YTT / SMT AMALGAMATION

Triassic

gray shale, siltstone and limestone

Permian - Triassic

SIMPSON LAKE GROUP

polymictic conglomerate, sandstone, siltstone, mafic and felsic volcanic rocks, limestone

SLIDE MOUNTAIN TERRANE

INTRUSIVE ROCKS

Early Permian

ultramafic and mafic intrusions

LAYERED ROCKS

Lower to Middle Permian

Gatehouse formation

limestone and quartzite

SLIDE MOUNTAIN TERRANE

Lower Permian

Campbell Range formation

basalt and varicolored chert

Carboniferous to Permian?

FORTIN CREEK GROUP

dark phyllite and chert, varicolored chert, chert-pebble conglomerate, sandstone, limestone, felsic and mafic metavolcanic rocks

YUKON-TANANA TERRANE

INTRUSIVE ROCKS

Late Devonian to Early Mississippian

SIMPSON RANGE PLUTONIC SUITE

granite, quartz monzonite, granodiorite

GRASS LAKES PLUTONIC SUITE

granite, quartz monzonite augen granite

ultramafic and mafic intrusions, Big Campbell and Cleaver Lake thrust sheets

LAYERED ROCKS

Lower Permian

Money Creek formation

dark phyllite and sandstone, chert, chert-pebble conglomerate, diamictite

Mid-Pennsylvanian to Lower Permian

Finlayson Creek limestone

massive bioclastic limestone

YUKON-TANANA TERRANE

Upper Mississippian to mid-Pennsylvanian

undifferentiated White Lake and King Arctic formations

green and pink chert, limestone, sandstone, conglomerate, mafic metavolcanic rocks

Upper Mississippian

Whitefish limestone

massive bioclastic limestone

Lower Mississippian

Tuchitua River formation

intermediate, felsic and mafic volcanic rocks, sandstone, chert, limestone

WOLVERINE LAKE GROUP

undifferentiated mafic and felsic volcanic rocks and dark clastic rocks

Upper Devonian to Lower Mississippian

Cleaver Lake formation

calc-alkaline basalt, rhyolite, chert and volcanic-derived sandstone

Waters Creek formation

felsic to intermediate metavolcanic rocks and carbonaceous phyllite

GRASS LAKES GROUP

undifferentiated mafic and felsic volcanic rocks and dark clastic rocks of the Fire Lake, Kudz Ze Kayah and Wind Lake formations

Pre-Upper Devonian

North River formation

quartzose metaclastic rocks, marble and non-carbonaceous pelitic schist

Fig. 2. *(Cont.)*

A

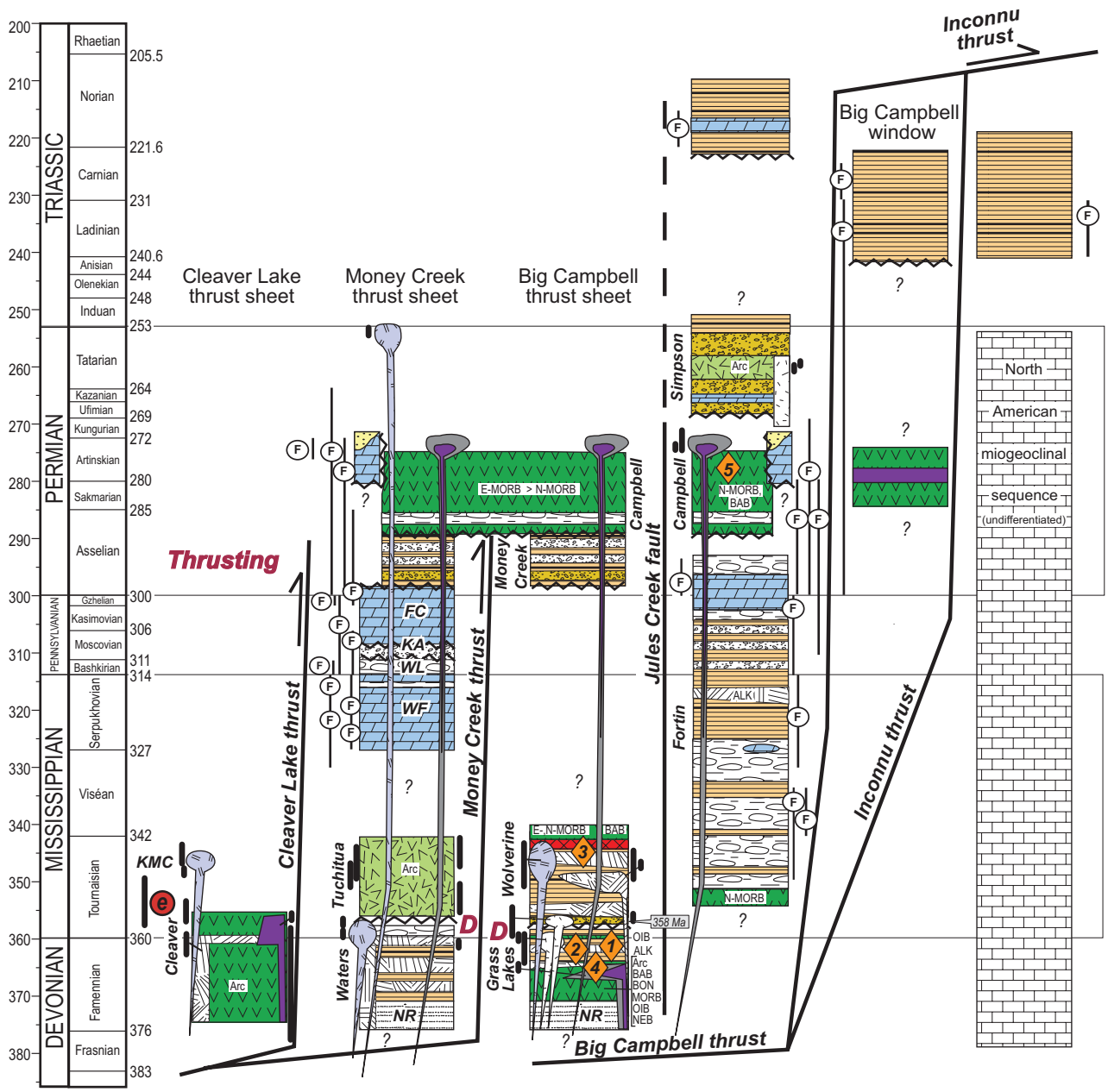

Protolith Lithologies

- Felsic intrusion
- Intermediate intrusion
- Mafic intrusion
- Basic volcanic rock
- Intermediate volcanic rock
- Felsic volcanic rock
- Volcaniclastic rock
- Conglomerate
- Grit
- Orthoquartzite
- Sandstone, siltstone
- Exhalite
- Chert, argillite
- Carbonaceous clastic rocks
- Limestone
- Ultramafic rock

Symbols

- Fossil age
- U-Pb age
- 358 Ma — Age of youngest detrital zircon
- Unconformity
- D — Deformation
- e — Eclogite

VMS Deposits

1. Kudz Ze Kayah
2. GP4F
3. Wolverine
4. Fyre
5. Ice

Petrogenetic Affinities

Arc	= island arc
BAB	= back-arc basin
BON	= boninite
N-MORB	= normal mid-ocean ridge basalt
OIB	= ocean island basalt
E-MORB	= enriched mid-ocean ridge basalt
NEB	= niobium-enriched basalt
ALK	= alkalic

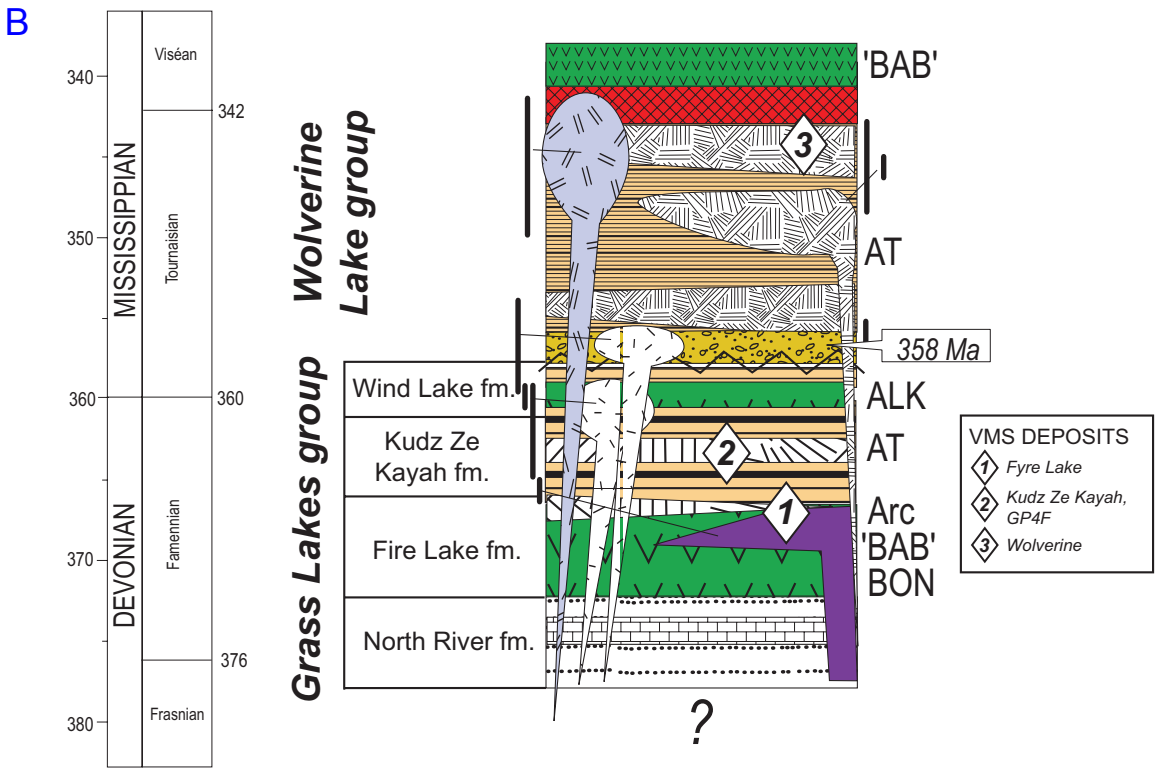

Fig. 3. Stratigraphic section illustrating relationships of different stratigraphic units in theYukon-Tanana terrane within the Finlayson Lake region. (A). All stratigraphic units within the Finlayson Lake region. (B). Detailed stratigraphy of Grass Lakes and Wolverine Lake groups. Abbreviations: ALK = alkaline basalt, Arc = basalts with arc affinity, AT = A-type felsic rocks, "BAB" = back-arc basin basalt, BON = boninite. Bars near plutons reflect range of U-Pb ages. Modified from Murphy et al. (2006) and Piercey et al. (2008).

iron formation (Figs. 4, 7; Peter et al., 2007). Shales are interlayered with the immediate footwall tuffs in the Fisher zone; some of the longer drill holes here extend hundreds of meters into the footwall and thus provide insights into the deepest parts of the VMS-hosting basin and ambient conditions in the basin prior to deposit formation. The stratigraphically lowest footwall shale is very carbonaceous and contains fine-grained pyrite (Figs. 7, 9). In the hanging wall, shales are broadly similar to those of the footwall, but interlayered with volcanic siltstone, carbonate exhalite, and volcanic breccia in the lower hanging wall, and with more mafic material in the uppermost hanging wall (e.g., Fig. 5).

The Sable zone occurs 1.6 km along strike and southeast of the Wolverine deposit and has a similar correlative stratigraphy (Figs. 4, 7). This zone has a footwall containing abundant felsic volcaniclastic rocks interlayered with carbonaceous shale, some of which have minor sphalerite-pyrite stringers (Fig. 7), and ~352 Ma quartz-K-feldspar porphyritic intrusions similar to those found at the Wolverine deposit (Piercey et al., 2008). Mineralization in the Sable zone comprises thin intervals of massive sulfide with strong quartz-pyrite-Fe carbonate alteration (Peter et al., 2007). The hanging wall consists of abundant volcanic siltstone interlayered with carbonaceous shale and iron formation, similar to the hanging wall in other zones of the deposit (Fig. 7), and has abundant quartz-sericite alteration and local magnetite proximal to magnetite iron formation.

The Puck zone is the southernmost mineralized zone on the Wolverine property, located ~6 km from the Wolverine deposit (Fig. 4). The Puck zone differs slightly from the other zones in having abundant mafic rocks within the stratigraphy (Fig. 7). Footwall strata there consist of variably interlayered felsic volcaniclastic rocks and carbonaceous shale that are variably altered to quartz, sericite, and chlorite (Figs. 7, 9). Locally, the footwall contains K-feldspar porphyritic intrusions like those in the Wolverine and Fisher zones (Piercey et al., 2008). Mineralization consists of sphalerite, chalcopyrite, and galena in stringer veins and massive sulfide, in variably sericite-altered quartz- and feldspar-rich tuffaceous rocks (Fig. 7). The immediate hanging wall comprises felsic volcanic siltstone interlayered with carbonaceous shale that grades upward into magnetite iron formation, with local carbonate exhalite (Fig. 7; see also Peter et al., 2007). The upper hanging wall consists of gabbro intrusions, and mafic dikes/sills interlayered with volcanic siltstone and carbonaceous shale. These mafic sills commonly exhibit peperitic margins with the surrounding shale.

Lithogeochemistry

Sampling and analytical methods

Samples of shale were collected from the Wolverine, Fisher, Sable, and Puck zones (Table R1). Samples were divided into those occurring in the footwall, within 10 m of mineralization, and above 10 m from mineralization but below the uppermost iron formation, and above the uppermost iron formation. This stratigraphic division was undertaken to examine variations in relationship to mineralization, but also to understand the

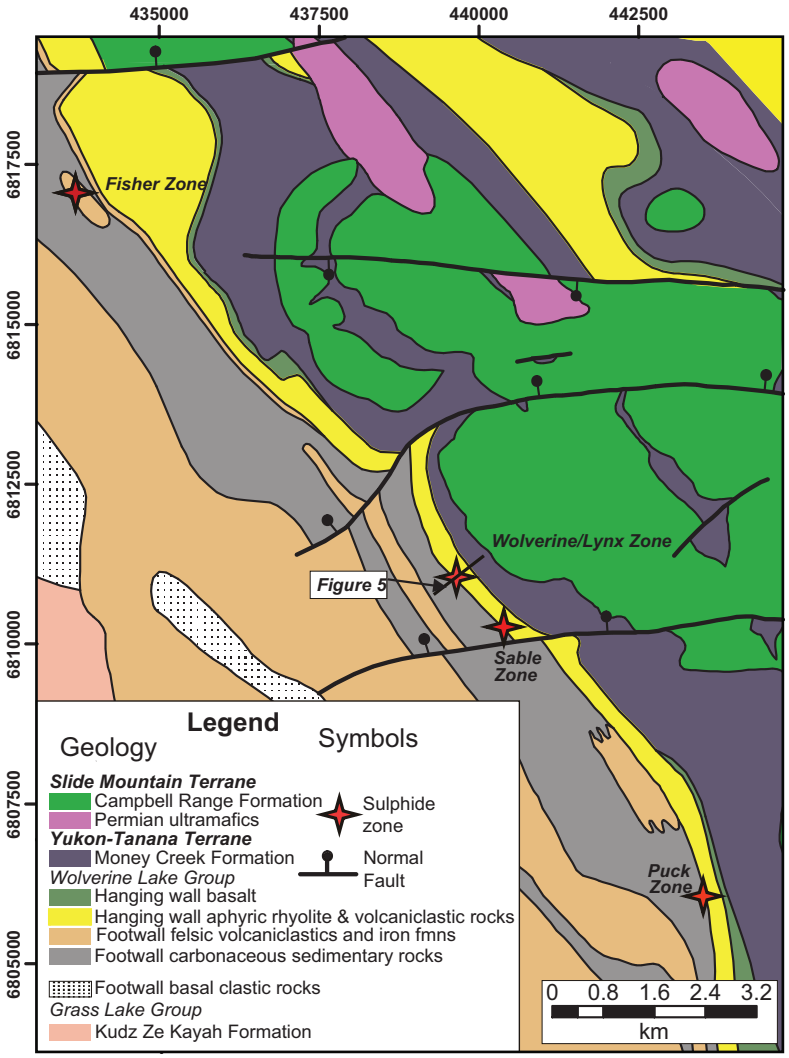

Fig. 4. Geology of local Wolverine deposit area, showing locations of different zones. Geology from Murphy et al. (2006).

ambient environment of formation outside of the immediate mineralized zones. In particular, unaltered samples from the very deep footwall of the Fisher zone that extend to hundreds of meters below mineralization provide insight into the background environment of formation at the onset of hydrothermal activity (i.e., ambient basinal conditions); those in the uppermost hanging wall record the ambient environment following Wolverine deposit formation. In contrast, samples of mineralized strata provide insight into the environment at the time of ore formation and record effects of hydrothermal activity on shales proximal to mineralization.

All samples were analyzed for major elements and certain trace elements (Zr, Nb, Y, Ga) via fused-disk X-ray fluorescence (XRF) and pressed-pellet XRF methods, respectively, at Activation Laboratories in Ancaster, Ontario (2005 samples) and at the Ontario Geoscience Laboratories in Sudbury, Ontario (2006 samples). Trace elements, including rare earth elements (REE), were determined by a combination of inductively coupled plasma-emission spectrometry (ICP-ES) and inductively coupled plasma-mass spectrometry (ICP-MS). Samples from 2005 were analyzed for trace elements and REE at the Ontario Geoscience Laboratories via closed-beaker acid digestion with a finish by ICP-ES and ICP-MS (Burnham et al., 2002; Burnham and Schweyer, 2004); samples from 2006 were analyzed via high-precision ICP-MS at the Chemical Fingerprinting Laboratory in the Department of Earth Sciences, Laurentian University, Sudbury, following the methods of Kamber (2009) and Marx and Kamber (2010). Solution ICP-MS results were compared to solid source results from pressed pellet XRF to ensure dissolution was complete using Zr as a proxy for the effectiveness of digestion of resistant phases, which is particularly critical for HFSE and REE (Fig. A1 in Data Repository). Zirconium was chosen because it yields very precise and accurate results by XRF, unlike Nb and Y by XRF in this dataset, which are at the limits of the XRF instrumentation for precision and accuracy. Given that all shale samples have a strong 1:1 correlation for Zr between ICP and XRF results (Fig. A1), it is reasonable to assume that dissolutions were complete using the closed beaker digestions (e.g., Burnham et al., 2002; Burnham and Schweyer, 2004; Kamber, 2009; Marx and Kamber, 2010). Due to the higher sensitivity and lower detection limits of the ICP-MS (vs. XRF)

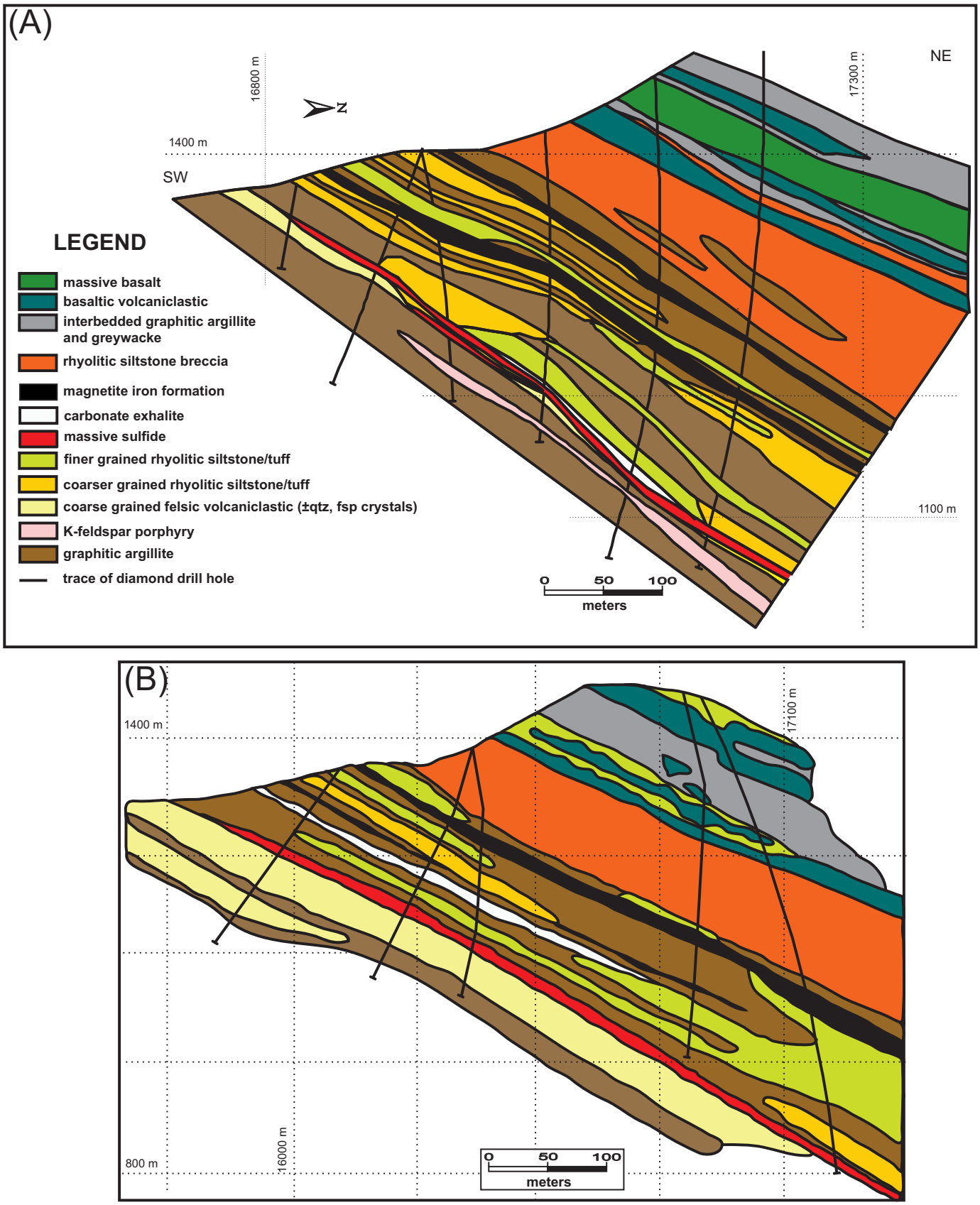

Fig. 5. Geologic cross sections through Lynx (A) and Wolverine (B) zones of Wolverine deposit. Locations of cross sections in the deposit are shown in Figure 8. Sections modified from Bradshaw (2003) and Bradshaw et al. (2008).

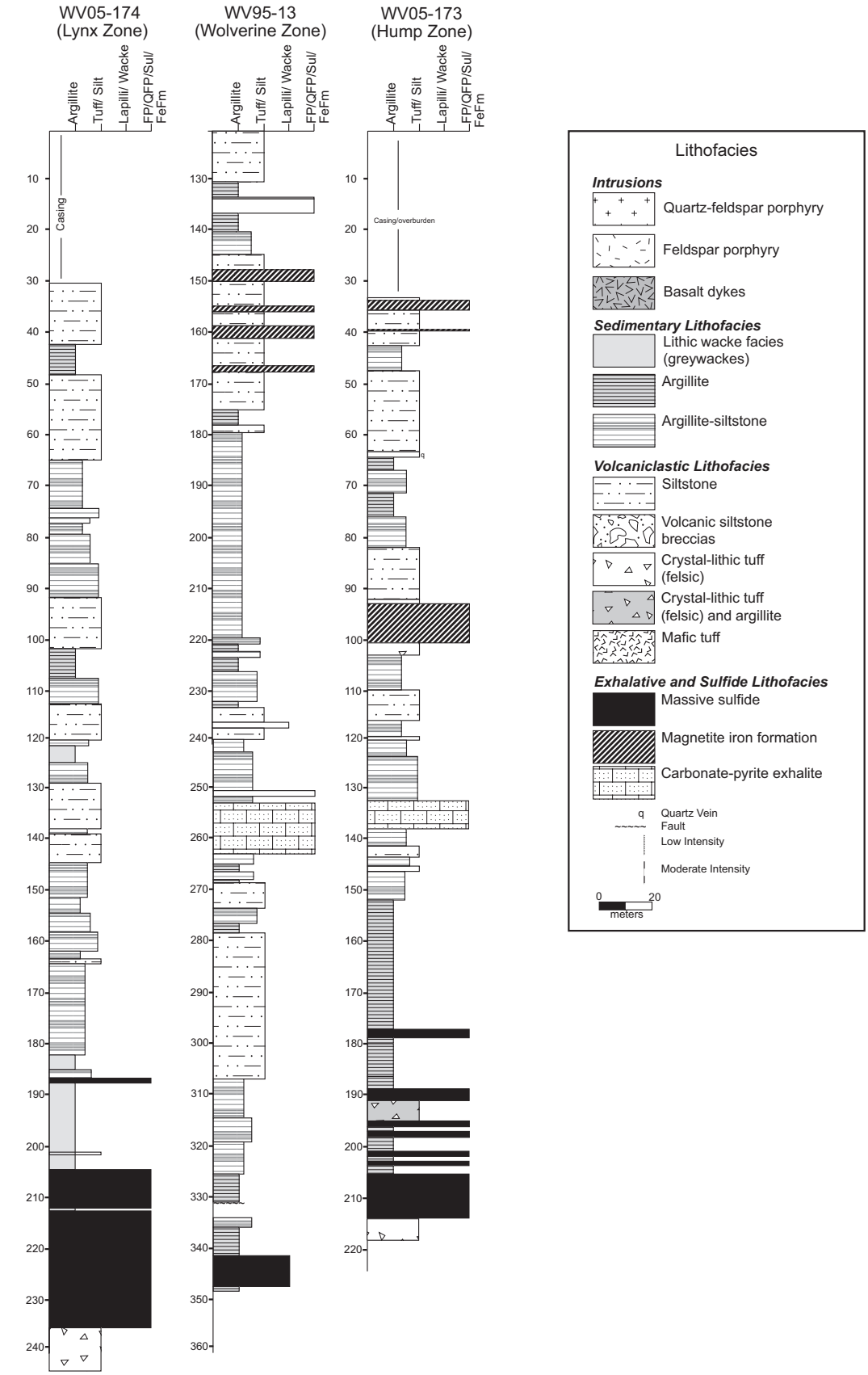

Fig. 6. Representative graphic logs of relationships of shales and other lithofacies to mineralization within the Wolverine, Lynx, and Hump zones. Location of drill holes shown in Figure 8.

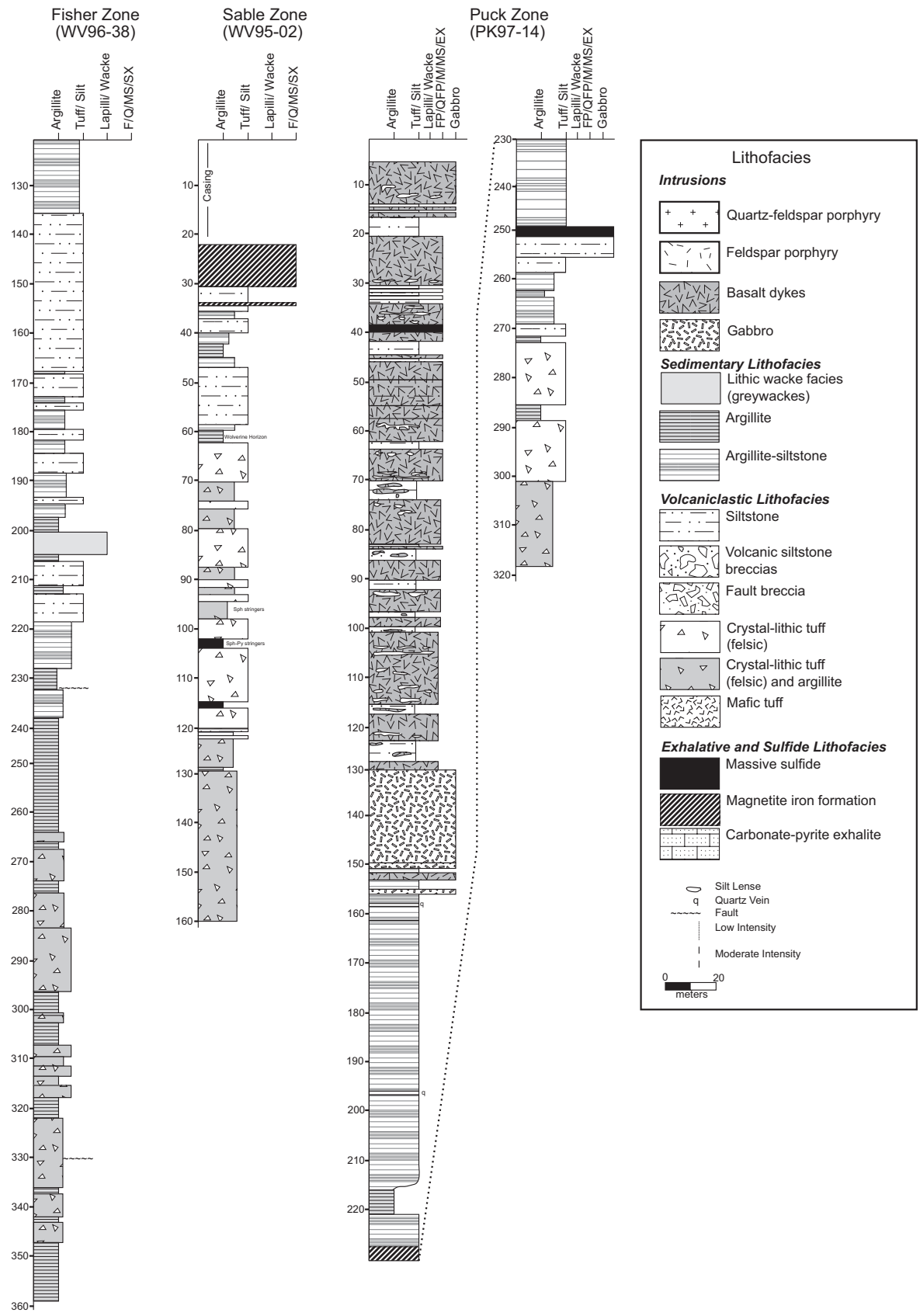

Fig. 7. Representative graphic logs of relationships of shales and other lithofacies to mineralization within the Fisher, Sable, and Puck zones. Location of drill holes shown in Figure 8.

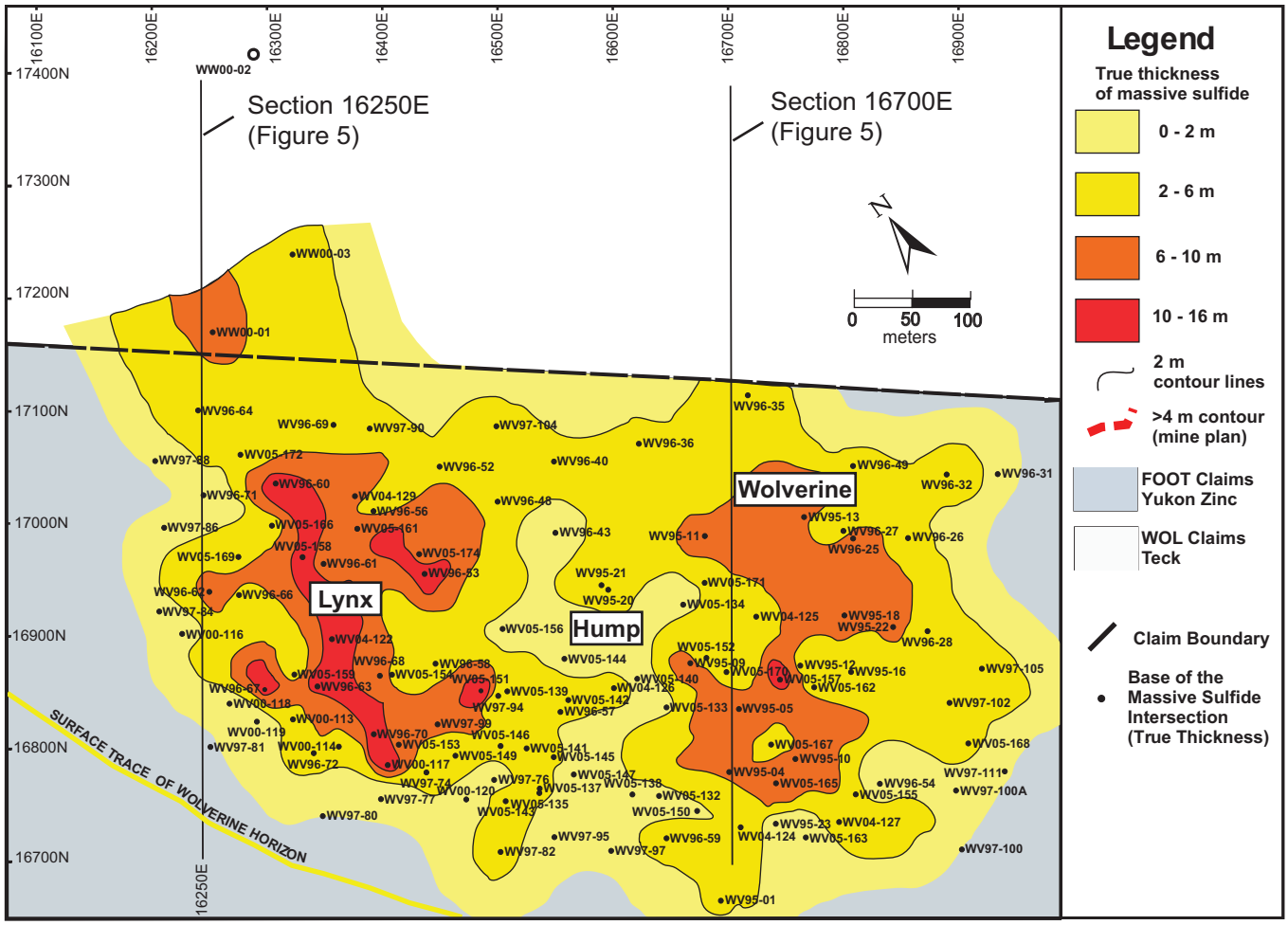

Fig. 8. Isopach map of mineralization thickness in Wolverine deposit and locations of cross sections and drill holes shown in Figures 5 through 7. Diagram modified from Pearson and Giroux (2006).

we have used HFSE and REE results from ICP-MS throughout this paper. Total CO_2 and S were analyzed via infrared spectroscopy, $C_{inorganic}$ was determined by Chittick methods (e.g., Brauneder et al., 2016), and $C_{organic}$ was determined via the difference in C_{total} (derived from total CO_2 and $C_{inorganic}$); all of the latter analyses were undertaken at the Ontario Geoscience Laboratories. Lithogeochemical results are presented in Table R1 in the Online Appendix.

Results

Major elements: Major element data for Wolverine shales are shown in Figure 10. On ternary plots that show the positions of various potential diagenetic and alteration minerals (Nesbitt and Young, 1984; McLennan et al., 1990; Nesbitt, 2003), data for Wolverine shales lie on a trend from illite/muscovite to calcite-dolomite in $(CaO + Na_2O)$-Al_2O_3-K_2O space, with low Al_2O_3 footwall samples plotting closer to the carbonate node (Fig. 10a). In $(CaO + Na_2O$-$K_2O)$-Al_2O_3-$(Fe_2O_3 + MgO)$ space, the samples lie within a triangular area between the muscovite, chlorite, and carbonate nodes (Fig. 10b). Wolverine shales have variable chemical indices of weathering values (CIW; Nesbitt and Young, 1984) with most samples having CIW >50 and with inverse trend with decreasing SiO_2/Al_2O_3. Samples with both low SiO_2/Al_2O_3 and CIW are those that plotted close to the carbonate nodes in Figure 10a-b.

Major and trace elements sensitive to hydrothermal overprint: In Fe-Mn-Al ternary space the shale compositions lie closer to the detrital portion of the diagram with very limited indication of hydrothermal input (Fig. 11a). On a Fe/Ti versus Al/(Al + Fe + Mn) plot, most Wolverine shales have a maximum of ~35% hydrothermal component and are dominated by detrital components; most samples exhibiting a greater hydrothermal input are from the Wolverine deposit area (Fig. 11b). Some shales also have elevated contents of Zn-Cu-Pb, and Tl and Sb; however, the majority of samples have Cu less than 200 ppm and Zn + Pb less than 1,000 ppm (Fig. 11c, d).

Redox-sensitive trace elements: The multiple-valence transition metals are typically controlled by aqueous basin redox or conditions at the sediment-water interface (Emerson and Huested, 1991; Calvert and Pedersen, 1993, 1996; Jones and Manning, 1994; Quinby-Hunt and Wilde, 1994; Algeo and Maynard, 2004, 2008; Tribovillard et al., 2006; Little et al., 2015). Most shale samples analyzed in this study have low Mn contents (<1,000 ppm), except those in the uppermost part of the stratigraphy that contain ca. 1,000 ppm and those having elevated CO_2 and CaO contents (Fig. 12a, b). Despite

Fig. 9. Various lithofacies of Wolverine deposit. (A). Footwall shales with felsic tuff along laminae. (B). Massive carbonaceous mudstone from deeper portions of Fisher zone. (C). Carbonaceous shales atop mineralization as well as remnant shale beds within the massive sulfide mineralization. These shales illustrate a replacement front into the shales near the massive sulfide-shale contact. (D). Hanging-wall carbonaceous shale interlayered with felsic tuffaceous material.

variations in Mn content, the V/(V + Ni) ratios for the shales plot within the anoxic field, with some exceptions (Fig. 12a). The elevated V is mirrored in high V/Cr ratios and elevated U/Th and Ni/Co ratios, with most data plotting in the anoxic to suboxic fields (Emerson and Huested, 1991; Hatch and Leventhal, 1992; Jones and Manning, 1994; Algeo and Maynard, 2004, 2008; Tribovillard et al., 2006); however, there is some scatter in U/Th (Fig. 12c, d) as discussed below. Molybdenum and U enrichment factors relative to Post-Archean Australian Shale [EF = $(X_{sample}/Al_{sample})/X_{PAAS}/Al_{PAAS}$], where X = Mo or U (Algeo and Tribovillard, 2009)] are shown in Figure 12e, demonstrating that most samples are highly enriched in these elements. Similarly, authigenic U (U_{auth} = U-Th/3) is also enriched in the Wolverine shales and shows a positive correlation with $C_{organic}$ content (Fig. 12f). Ratios of sulfur to organic carbon are mostly greater than 0.32 (Fig. 12g). The elevated S values are affected by sulfide mineralization, but even those screened for sulfide mineralization (e.g., Fe_2O_3 <5 wt %, Zn <200 ppm, Cu <200 ppm) have $S/C_{organic}$ >0.32 (Fig. 12h).

Variations in trace element concentrations are also shown stratigraphically in Figure 13. Notable is that shales in the uppermost hanging wall above mineralization have the highest Mn, and low S, $C_{organic}$, and U-Mo-V, similar to results outlined above. Similarly, the deeper footwall shales have low Mn, but more variable S and $C_{organic}$ contents, and generally low U-Mo-V (Fig. 13). In contrast, shales proximal to mineralization have low Mn, and elevated S, $C_{organic}$, Zn, and U-Mo-V.

Rare earth element and yttrium (REY) systematics: The REE are particularly useful for understanding redox conditions in shales (e.g., de Baar et al., 1988; Elderfield et al., 1988), and when coupled with data for Y are also sensitive indicators of potential inputs from oxygenated seawater (e.g., Bau, 1996). Patterns of REY normalized to average Post-Archean Australian Shale (PAAS; McLennan, 1989) for the shales analyzed herein are shown in Figure 14. To aid analysis of these plots, the samples are broken out based on both stratigraphic setting and similarity of REY signatures. In the deepest footwall shales from the Fisher zone and the uppermost shales in the Wolverine area (above the iron formations), the signatures are remarkably similar, and display very flat patterns that have no or small negative Ce anomalies (i.e., Ce/Ce* ~1; Fig. 14a, b). Samples from the immediate footwall of the Wolverine deposit also have flat patterns, but with more pronounced negative Ce anomalies (Ce/Ce* <1), small positive Y anomalies (i.e., elevated Y/Ho), and no or small negative Eu anomalies (Fig. 14c). A similar pattern is found in shales in the immediate hanging wall to mineralization; however, the range of total REY abundances, and the magnitudes of the

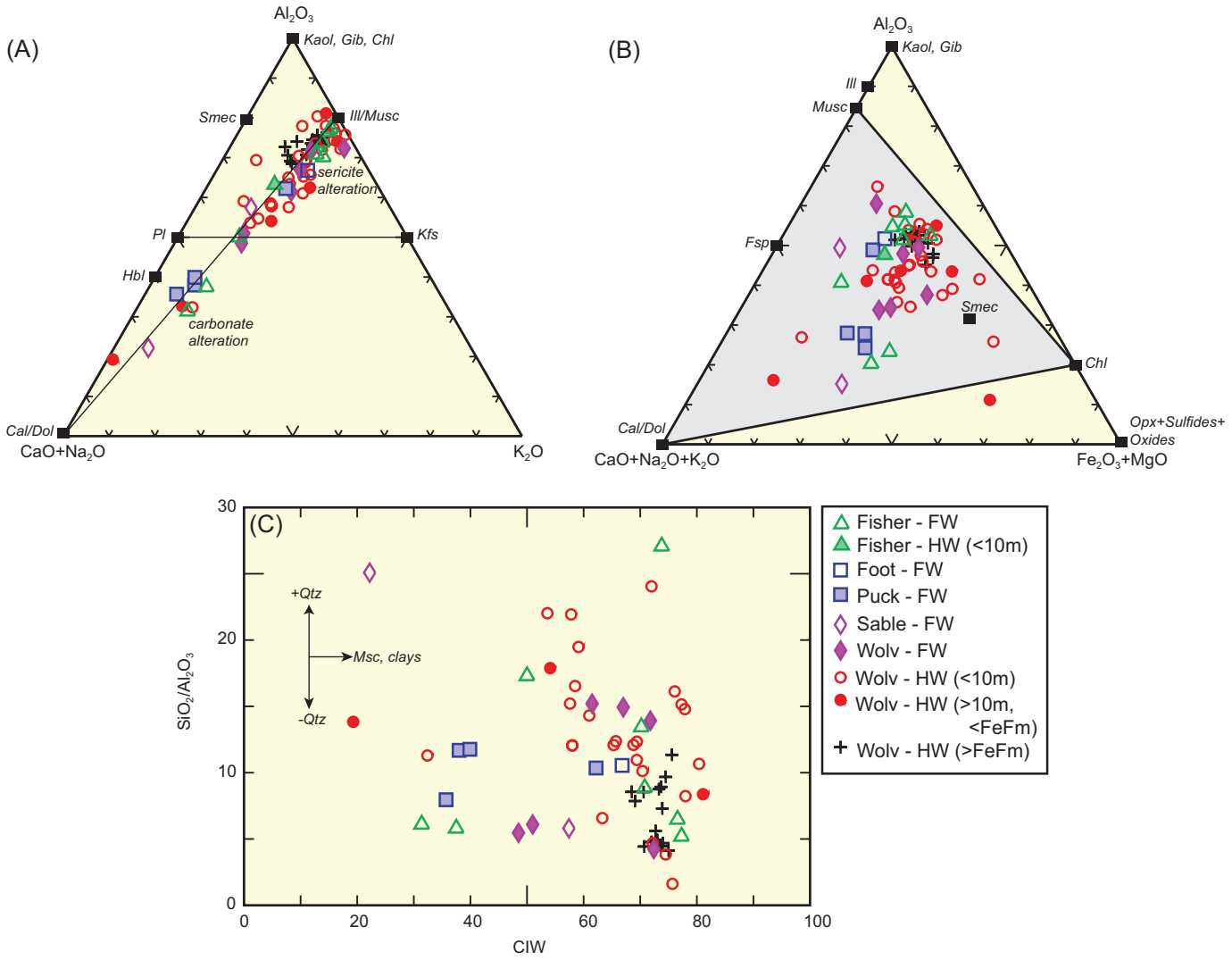

Fig. 10. Major element plots for Wolverine shales. (A). Ternary CaO + Na_2O vs. Al_2O_3-K_2O and (B) CaO + Na_2O + K_2O-Al_2O_3 vs. Fe_2O_3 + MgO plots after Nesbitt and Young (1984) and Nesbitt (2003). (E). SiO_2/Al_2O_3 (measure of silicification) vs. chemical index of weathering (CIW; measure of clay mineral abundance and feldspar destruction). CIW formula from Nesbitt and Young (1984).

Eu, Ce, and Y anomalies are variable (Fig. 14d). Shale samples that are 10 m stratigraphically above mineralization, but below the iron formation, also display patterns similar to those of the immediate Wolverine hanging wall, with the exception of one sample that is silicified and has very low total REY contents (Fig. 14e). The Puck zone shales have signatures similar to those of shales in the immediate Wolverine hanging wall, characterized by uniformly flat to weakly light rare earth element (LREE)-depleted signatures with negative Ce and Eu anomalies and positive Y anomalies (Fig. 14f).

The REY systematics are further evaluated in Figure 15 to understand the significance of Ce and Y anomalies. Because a negative Ce anomaly on a PAAS-normalized plot can be caused by a deficit of Ce and/or an excess of La (Bau and Dulski, 1996; Kamber and Webb, 2001) a test is required to estimate both influences. This test involves plotting the Ce anomaly against the apparent Pr anomaly. Given that all shales from the Wolverine deposit have $Ce/Ce^* \leq 1$ and $Pr/Pr^* > 1$, these samples thus have true negative Ce anomalies and also mild positive La anomalies (Fig. 15a). The Ce/Ce^* anomalies also exhibit a weak anticorrelation with P_2O_5 contents (Fig. 15b); however, all samples with negative Ce anomalies have elevated P_2O_5 contents (i.e., >0.05% P_2O_5).

The Y/Ho systematics for the Wolverine shales vary and range from values that are chondritic and rock-like (~27) to much higher values that are similar to seawater (~44), and they are clusters, but some of the lower values of Y/Ho correlate with negative Ce anomalies, and increasing Pr/Pr^* (Fig. 15c, d).

The REY systematics are also shown in downhole form in Figure 13. In the immediate area of sulfide mineralization, shales have remarkably low Ce/Ce^* values less than 1; there are also elevated Y/Ho at this location as well (Fig. 13). Although the latter element ratios do show spikes elsewhere in the stratigraphy, they are not as pronounced as near mineralization.

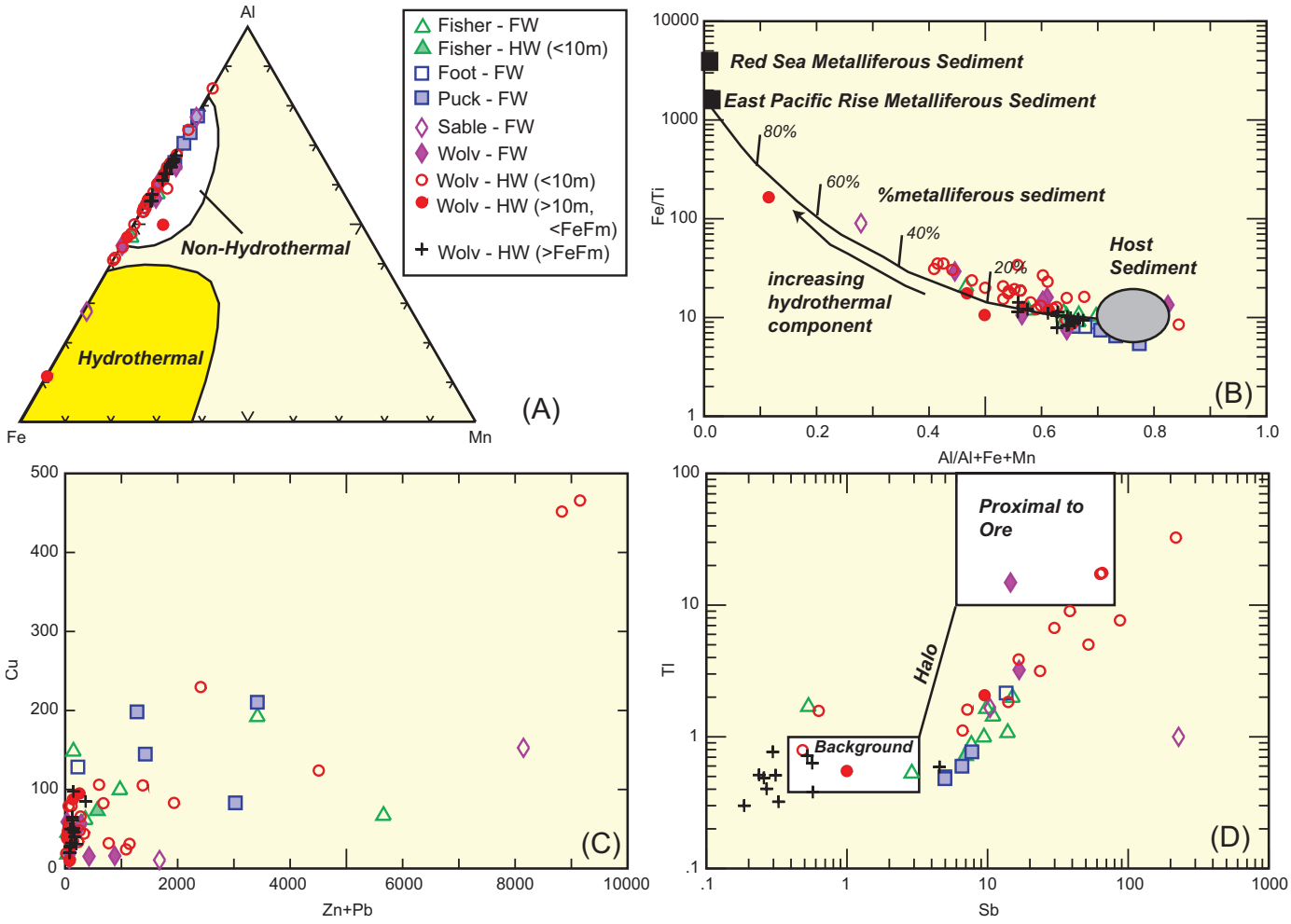

Fig. 11. Hydrothermal element provenance plots. (A). Fe-Al-Mn ternary plot. (B). Fe/Ti vs. Al/(Al + Fe + Mn) plot (Boström, 1973). (C). Cu vs. Zn + Pb. (D). Tl vs. Sb plot after Large et al. (2001).

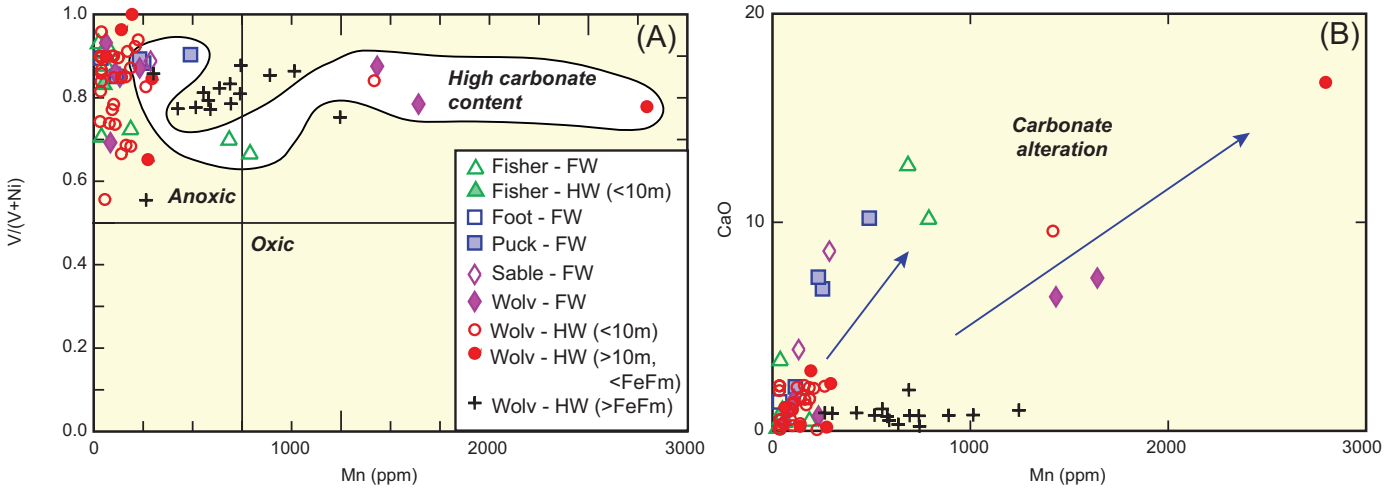

Fig. 12. Redox-sensitive trace element plots. (A). V/(V + Ni) vs. Mn. (B). CaO vs. Mn. (C). U/Th vs. V/Cr. (D) Ni/Co vs. V/Cr. (E) U_{EF} vs. Mo_{EF} (from Algeo and Tribovillard, 2009). (F). U_{auth} vs. $C_{organic}$. (G). S vs. $C_{organic}$. (H). S vs. $C_{organic}$ screened for samples with Fe_2O_3 <5 wt % and Zn <200 ppm. S vs. C_{org} (from Berner, 1984). Other references to redox-sensitive elements and ratios provided in text.

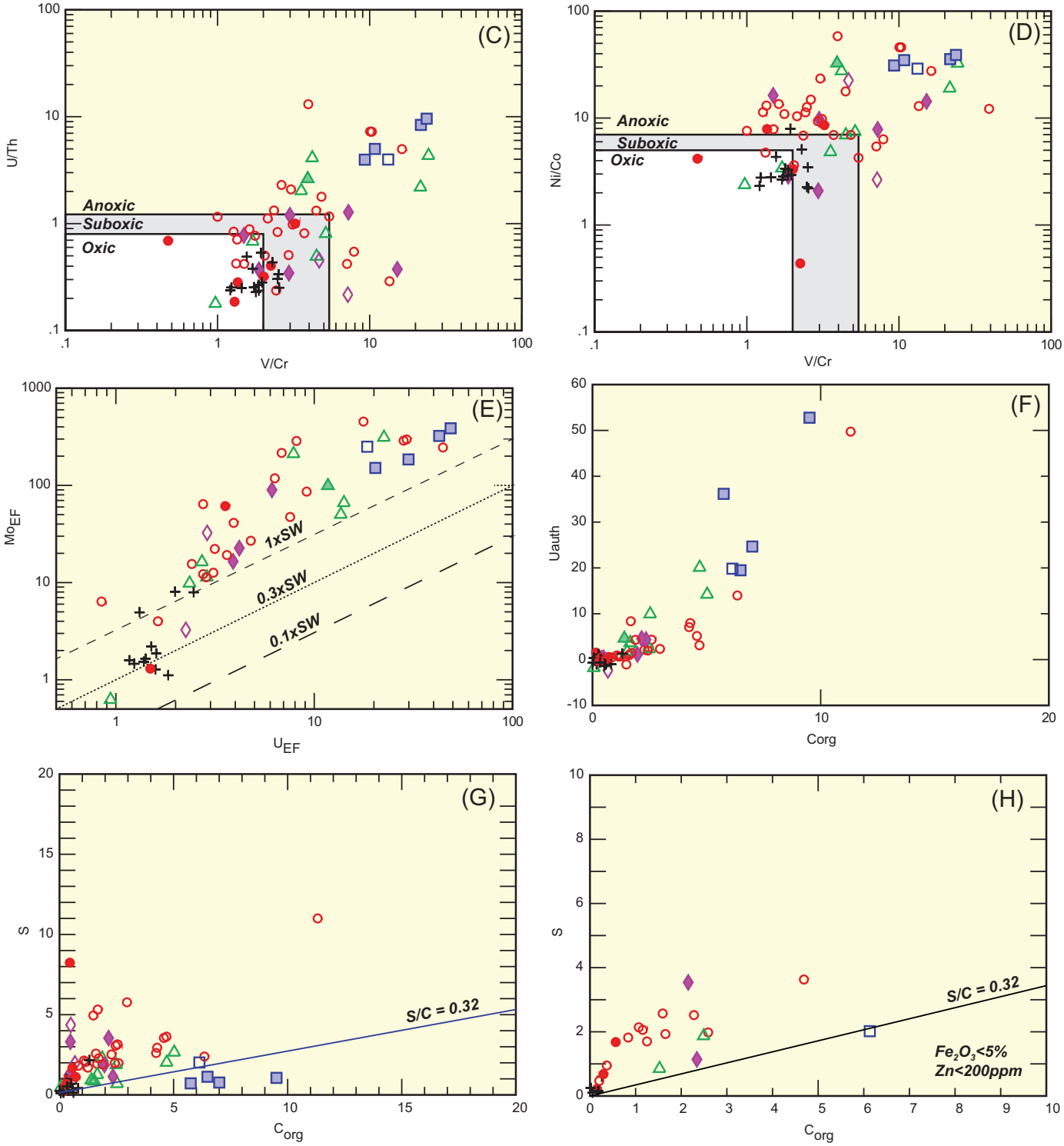

Fig. 12. *(Cont.)*

Discussion

Ambient redox environment

The ambient redox environment and oxygenation conditions of bottom waters have been cited in previous studies as exerting a first-order control on the formation and localization of some massive sulfide deposits (Goodfellow, 1987; Eastoe and Gustin, 1996; Goodfellow and Peter, 1996; Goodfellow et al., 2003b; Tornos et al., 2008; Menor-Salvan et al., 2010; Sáez et al., 2011). Many workers argue that in anoxic basins that reach euxinia, a stratified water column develops with an upper oxygenated and sulfate-rich layer

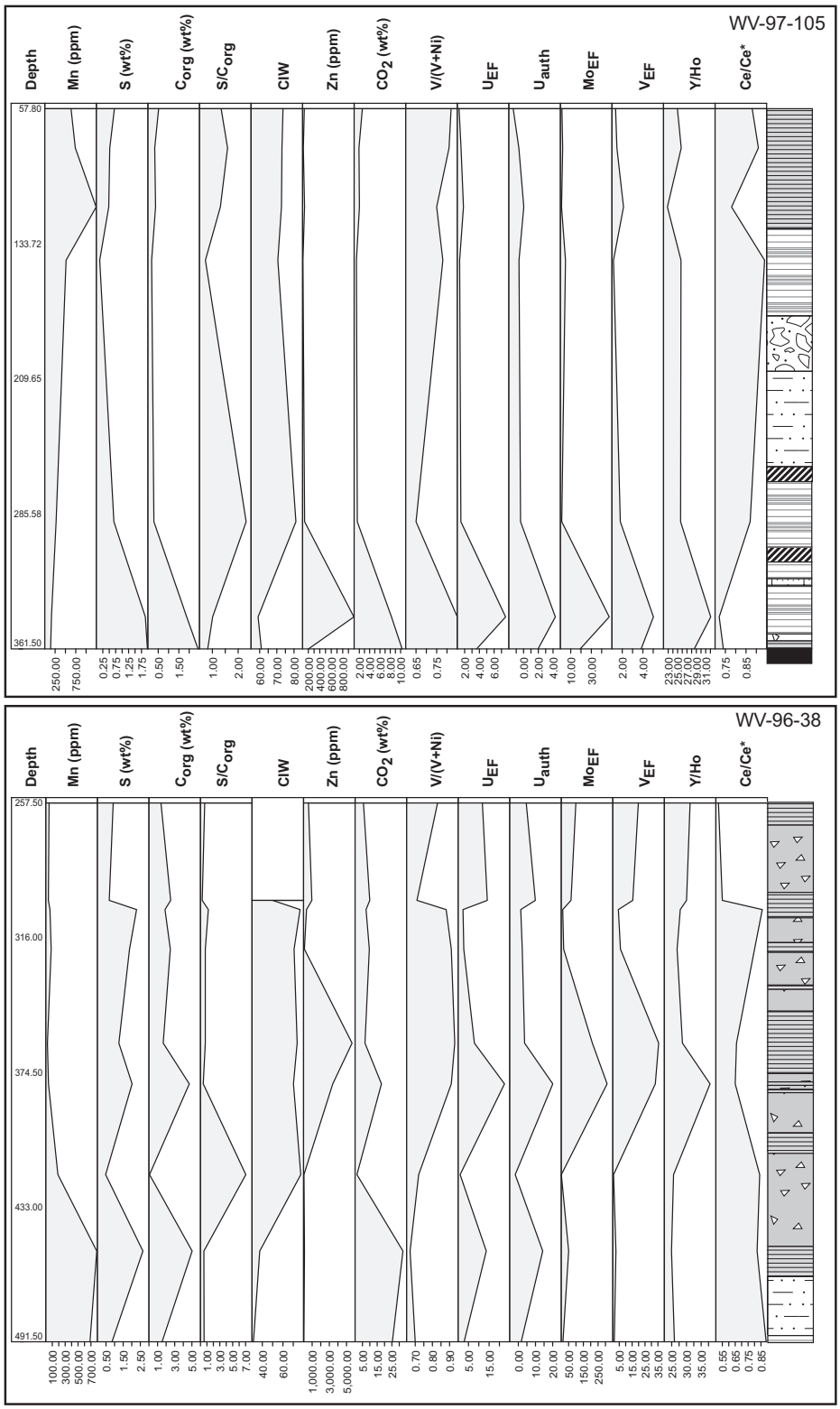

Fig. 13. Downhole profiles of key elements and element ratios with associated lithofacies. Drill Hole WV97-05 represents complete stratigraphic section of hanging wall to mineralization; WV96-38 is deepest hole into footwall.

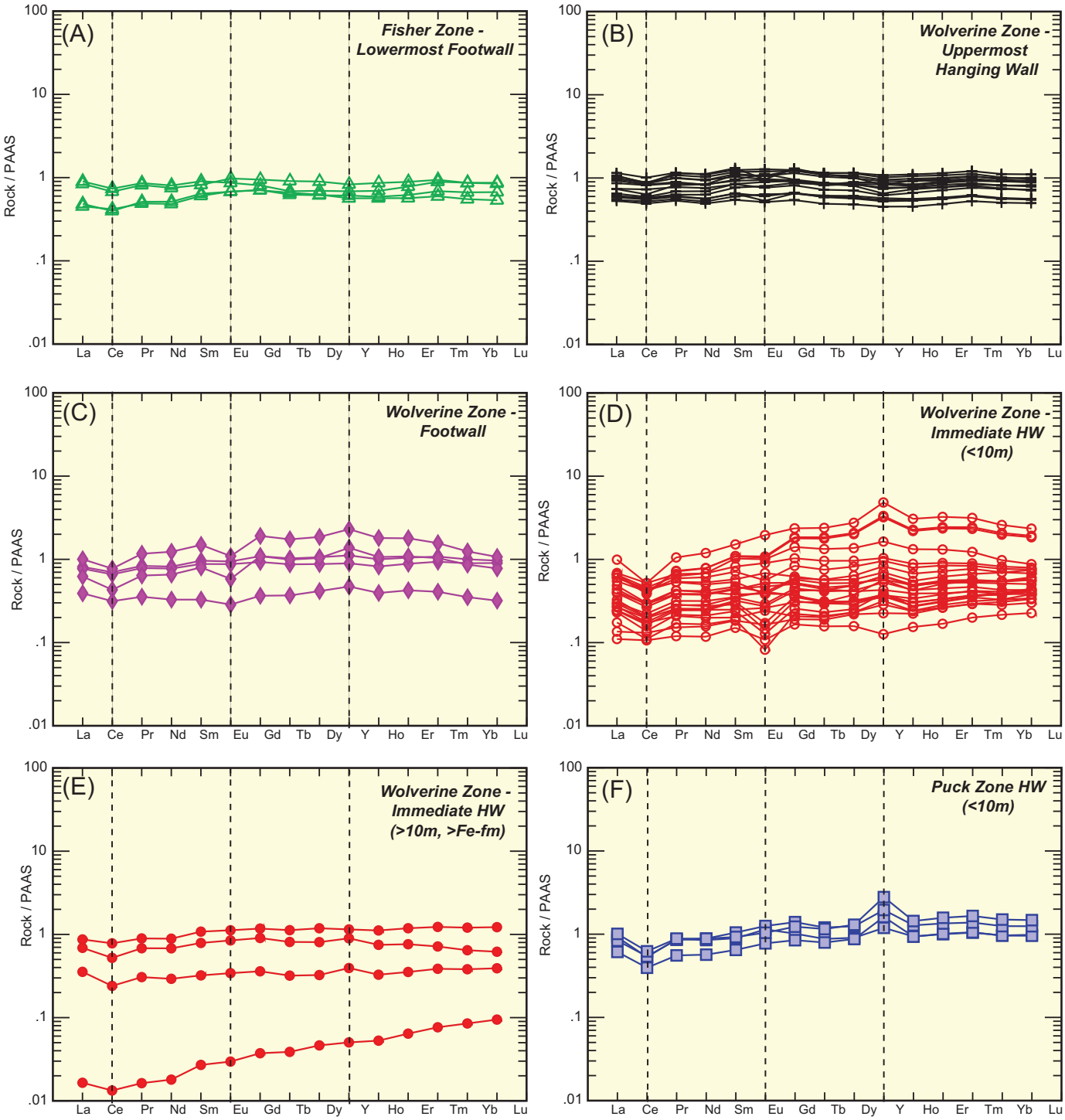

Fig. 14. Rare earth element and Y (REY) plots for various shale samples from the Wolverine deposit normalized to average Post-Archean Australian Shale (PAAS; normalization values from McLennan, 1989). (A). Fisher zone—lowermost footwall. (B). Wolverine zone—uppermost hanging wall. (C). Wolverine zone—footwall. (D). Wolverine zone—intermediate hanging wall. (E). Wolverine zone—intermediate hanging wall. (F). Puck zone hanging wall.

that is underlain by a suboxic to anoxic layer with variable amounts of free H_2S (euxinic; e.g., Leventhal, 1983; Raiswell and Berner, 1985; Goodfellow, 1987; Scott and Lyons, 2012). Furthermore, throughout Earth history there is a broad secular correlation between large tonnages of massive sulfide (e.g., Bathurst, Iberian pyrite belt) and global anoxic ocean events (e.g., Goodfellow et al., 2003b), which are linked via the more efficient complexing of metals in vent fluids with free H_2S in the bottom waters and precipitation of metal sulfides on the seafloor, coupled with the insulation of sulfide

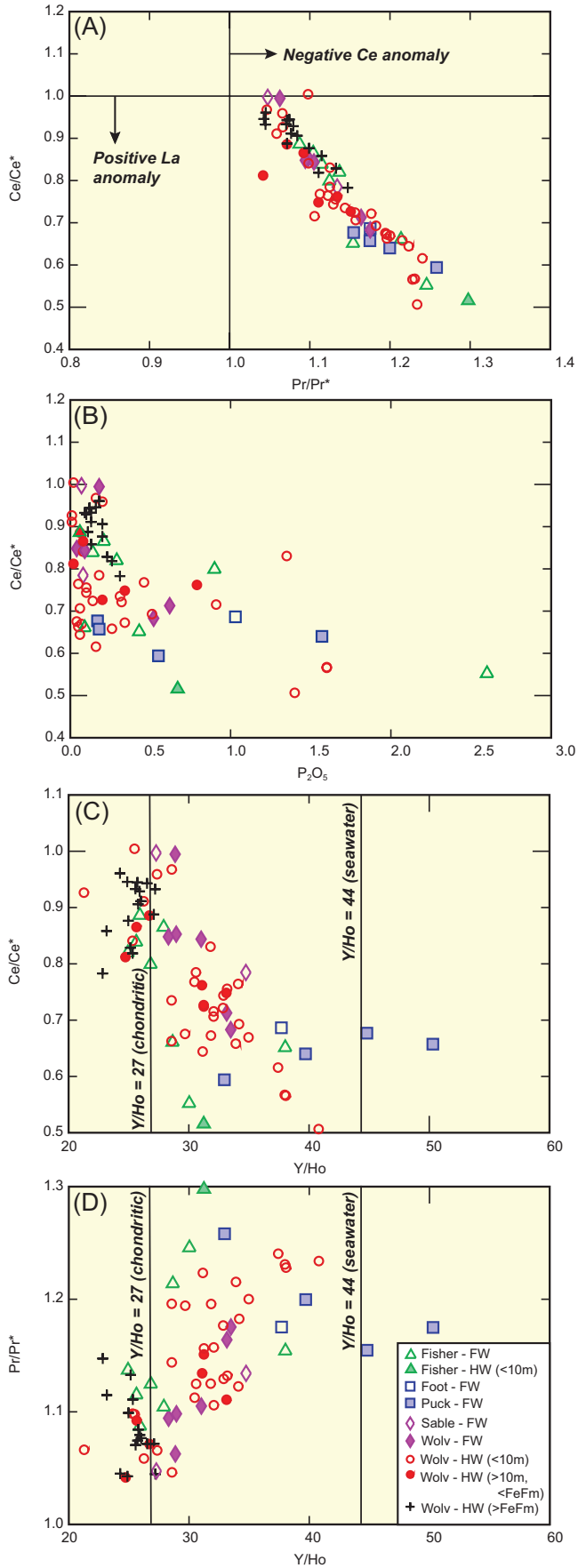

Fig. 15. REY systematics of Wolverine shales. (A). Ce/Ce* vs. Pr/Pr* plot of Kamber and Webb (2001), illustrating true negative Ce anomalies and positive La anomalies. (B). Ce/Ce* vs. P_2O_5, illustrating weak negative correlations with P_2O_5. (C). Ce/Ce* vs. Y/Ho plot, illustrating a decrease in Ce anomaly coincident with an increase in Y/Ho. (D). Pr/Pr* vs. Y/Ho. Y/Ho ratios for reservoirs are converted to element ratio from Bau (1996).

mounds from oxidation and seafloor weathering by oxygenated seawater (e.g., Eastoe and Gustin, 1996; Goodfellow and Peter, 1996; Goodfellow et al., 2003b).

To constrain the ambient redox conditions of the Wolverine shales, a multiproxy approach has been taken. This was done in recognition of the fact that certain redox proxies are more reliable than others (e.g., Tribovillard et al., 2006; Little et al., 2015). The combined approach shows that the majority of proxies, including low Mn; elevated $S/C_{organic}$ ratios; elevated V contents, V/(V + Ni) and V/Cr ratios; and enrichments in U and Mo, suggest that most Wolverine shales were deposited under anoxic to suboxic/dysoxic conditions (Fig. 13; Berner and Raiswell, 1983; Raiswell and Berner, 1985; Emerson and Huested, 1991; Hatch and Leventhal, 1992; Calvert and Pedersen, 1993, 1996; Quinby-Hunt and Wilde, 1994; Algeo and Maynard, 2004, 2008; Tribovillard et al., 2006). Evidence for anoxia, however, does not necessarily imply that the basin was euxinic (sulfidic) with aqueous H_2S present in the water column. The $S/C_{organic}$ ratios of most samples are a very strong indicator of excess sulfur in the water column and hence euxinic conditions (e.g., Berner and Raiswell, 1983; Berner, 1984). However, this ratio can be affected by sulfide addition associated with mineralization, a high probability in the Wolverine deposit area, especially proximal to massive sulfide. Scott and Lyons (2012) showed that in ancient shales Mo contents >100 ppm are typical of euxinic conditions with free H_2S in the water column, those having less than 25 ppm but greater than 1 to 2 ppm (crustal average) reflect H_2S presence only in sediment pore waters, and those between 25 and 100 ppm are ambiguous. In the case of the intermediate range of Mo contents (25–100 ppm), it could reflect periodic H_2S in the water column, and/or variable Mo content of the water column due to reservoir effects, and/or dilution by high sedimentation rates (Scott and Lyons, 2012). The Mo concentrations observed for the Wolverine deposit shales show a considerable variation as a function of stratigraphic position, with samples from the footwall and hanging wall having average values <25ppm, particularly so for the uppermost hanging wall (Fig. 16). The footwall and immediate hanging wall, despite having average values <25 ppm, are highly variable with many samples having concentrations >100 ppm Mo (Fig. 16). The absolute Mo contents are therefore consistent with at least periodic H_2S presence in bottom waters during deposition of the footwall and immediate hanging-wall shales, and with suboxic to oxic conditions during deposition of the upper hanging-wall shales.

The Mo variation shown in Figure 16 likely is influenced by sedimentation rate and dilution, however, given that most shales are interlayered with volcaniclastic rocks, including felsic tuff beds (e.g., Figs. 6, 7, 9). To remove the potential effects of sediment dilution on the Mo signature, and to decipher whether the Wolverine basin did have free H_2S, Mo_{EF}

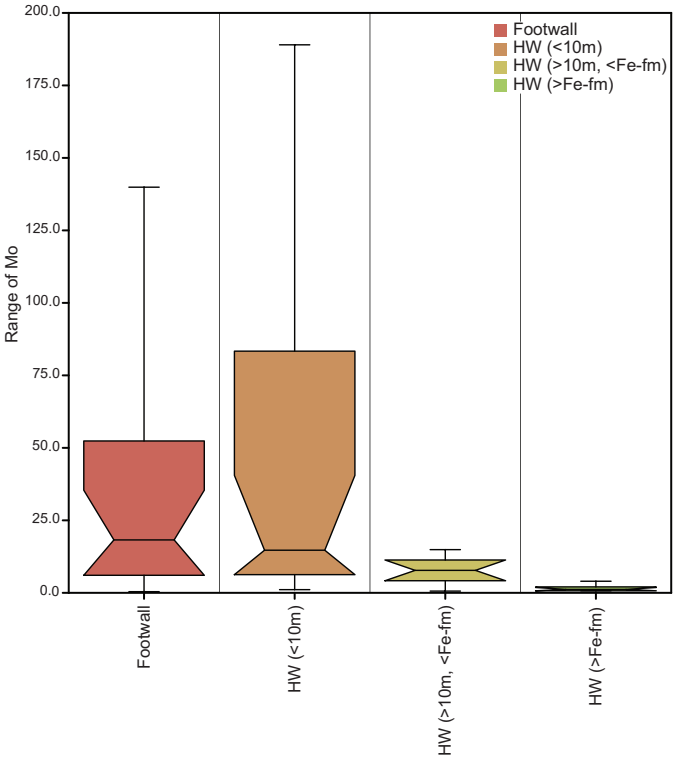

Fig. 16. Box and whisker plot of Mo concentrations in shales from the Wolverine deposit. Samples from footwall and immediate hanging wall have averages of less than 25 ppm, but include many that extend to concentrations above 100 ppm, indicative of euxinic conditions (see Scott and Lyons, 2012). In contrast, shales from upper hanging wall are less enriched and mostly have low Mo (<25 ppm). See text for discussion.

(and U_{EF}) systematics are utilized as they take into account potential dilution by detritus. Algeo and Tribovillard (2009) demonstrated that authigenic U enrichment will occur in anoxic basins with or without free H_2S; however, Mo enrichment will only occur if there is free H_2S in the water column. The Mo_{EF}-U_{EF} covariation diagram shows that the majority of shales from Wolverine have Mo-U systematics that are highly enriched relative to modern seawater, with those having lower Mo-U enrichments occurring mainly in the hanging wall, particularly in the upper part of the stratigraphy (Fig. 12e). This pattern is also seen in Figure 13, where Mo_{EF} and U_{EF} values are very high in the hanging wall above mineralization, are more erratic in the footwall but generally decrease with depth, and are very low in the upper hanging wall. The presence of such high Mo_{EF} values, particularly in footwall and hanging-wall samples proximal to mineralization, suggests that free H_2S existed in the water column and that the basin was at least periodically euxinic, particularly during VMS formation (e.g., Fig. 13; Algeo and Tribovillard, 2009; Little et al., 2015).

Both Mo and U show enrichment in Mo_{EF}-U_{EF} space; however, the pattern has a general flatness with higher U_{EF} values at a given Mo_{EF} (Fig. 12e). This distribution has been attributed to formation in a restricted or silled basin by previous workers (Algeo and Tribovillard, 2009). In these environments without periodic recharge of oxic ocean water, an excess of U develops relative to Mo, resulting in a reservoir effect whereby Mo is deposited initially and is then rapidly depleted from the water column, while U continues to be deposited after Mo is depleted (Algeo and Tribovillard, 2009). Data on the Mo_{EF}-U_{EF} array imply the possibility that the Wolverine deposit formed in a restricted to silled basin, consistent with regional tectonic models for the evolution of the ancient Pacific margin of North America where the Wolverine basin formed during rifting of the distal edge of the craton in the mid-Paleozoic (Nelson et al., 2006, 2013; Piercey et al., 2006; Colpron and Nelson, 2009). A restricted/silled basin on the edge of the craton would be an ideal location to deposit biomass from the continent (e.g., nutriet trap of Meyer and Kump, 2008), and create an environment that was deprived in O_2 and rich in H_2S. In particular, lack of oxygenation by influx of oxic seawater coupled with organic matter abundance would have provided an excess of electron donors to facilitate the biogenic reduction of seawater sulfate to H_2S and concentration of H_2S within the water column (Menor-Salvan et al., 2010). Support for organic matter buildup is illustrated in Figure 17, where a strong correlation is shown between organic C and Ni, an element that is indicative of productivity in the water column (Tribovillard et al., 2006; Little et al., 2015). Furthermore, the abundance of P_2O_5 in all shale samples (generally >0.05% P_2O_5) is also consistent with enhanced productivity and organic preservation in the Wolverine basin (e.g., Piper, 1994, 2001; Meyer and Kump, 2008; Piper and Calvert, 2011). Thus, it appears that the tectonics and restriction of the Wolverine basin, coupled with primary productivity, were critical in creating euxinia and an abundance of H_2S that was utilized for the formation of the Wolverine deposit (Fig. 18).

Basin restriction and euxinic conditions must have waned during evolution of the Wolverine basin as there are important stratigraphic variations in redox-sensitive trace elements. Most notably, samples from the upper hanging wall, above the iron formations, have higher Mn contents, and lower V contents, Mo_{EF}, U_{EF}, U_{auth}, and $S/C_{organic}$ ratios (Figs. 12, 13, 17), indicating a shift toward suboxic to oxic conditions during the

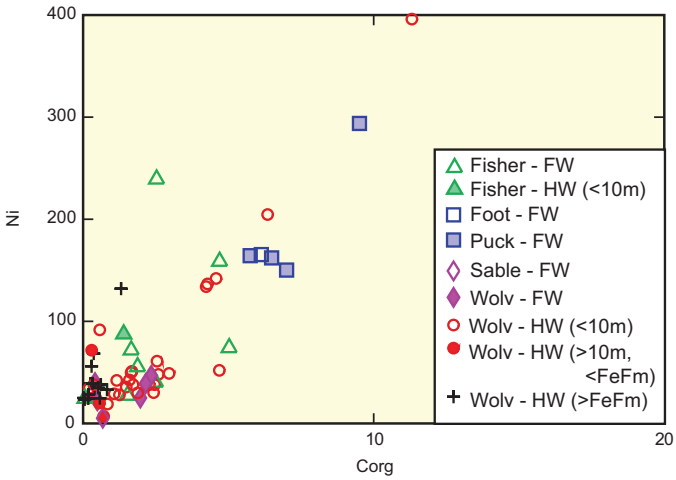

Fig. 17. $C_{organic}$ vs. Ni plot illustrating covariation of organic carbon and Ni. Elevated contents of both elements are indicative of enhanced primary productivity and preservation of organic carbon in parts of the Wolverine basin during sulfide mineralization.

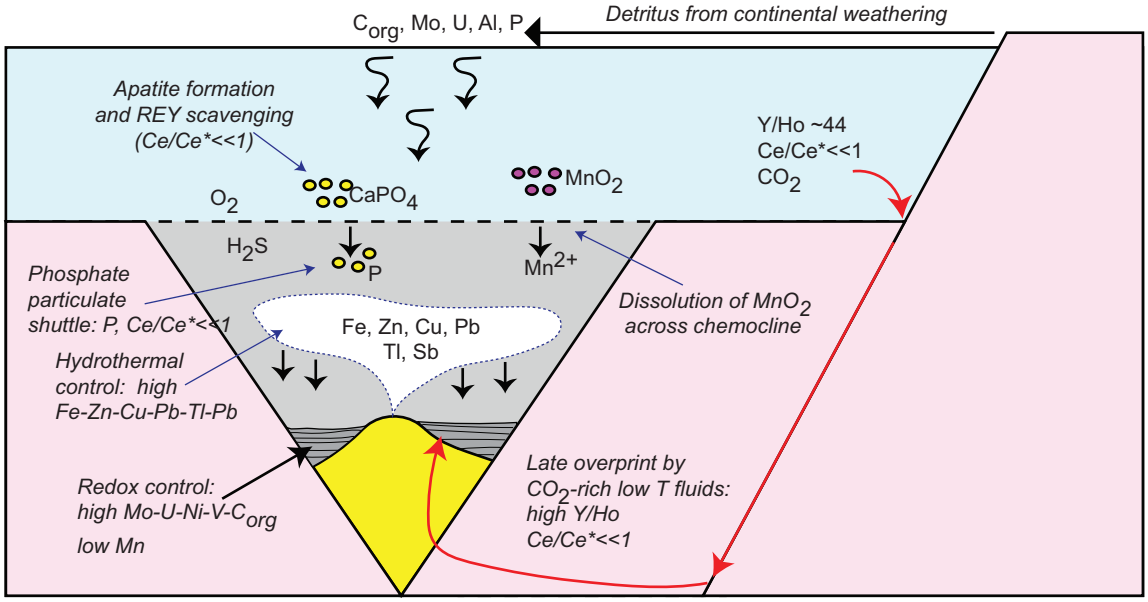

Fig. 18. Model for ambient basinal environment of Wolverine deposit with various chemical fluxes shown. Restricted nature of basin coupled with high organic productivity leads to deoxygenation of water column and generation of abundant aqueous H_2S. The H_2S formed during this process is utilized during genesis of the Wolverine deposit. The process also leads to shales enriched in redox-sensitive trace element suite Mo-U-Ni-V and depleted in Mn, the latter remaining in solution in the basin due to reducing conditions. Shales are also enriched in elements derived from hydrothermal venting, including Fe, base metals, and volatile elements. The REY are controlled, in part, by the scavenging of REE with low Ce/Ce* from oxygenated seawater during apatite formation upper water column and subsequent deposition as detrital grains into deeper waters. They are also affected by late overprinting by low-temperature, CO_2-rich seawater-rich(?) hydrothermal fluids resulted in elevated Y/Ho and Ce/Ce* <<1 in vent-proximal shales.

deposition of hanging-wall strata. The continued extension of the Wolverine basin and eventual formation of the Slide Mountain Ocean (back-arc basin; Nelson et al., 2006; Piercey et al., 2004, 2006) would have resulted in the ingress of oxygenated ocean waters as well as changing the geometry of the rifted margin, potentially destabilizing the existing nutrient trap, both of which would have shifted basin redox conditions from euxinic to oxic/suboxic (e.g., Figs. 12, 13, 17).

Collectively, the results above illustrate that the Wolverine basin had varying redox states, but that euxinia was important at least during deposit formation when H_2S was periodically present in the water column and contributed to the sulfur budget of the deposit (Fig. 18; Peter et al., 2007; Bradshaw et al., 2008). Euxinia was likely achieved via high productivity and physical restriction of the water column from oxic seawater in a silled basin/nutrient trap (Fig. 18), but as the basin evolved these conditions were interrupted and the basin shifted towards suboxic to oxic bottom waters due to ingress of oxygenated seawater during the development of a back-arc basin.

Rare earth element and Y (REY) systematics: overprint by oxygenated seawater?

REY systematics of the Wolverine shales show features that broadly parallel those of the redox-sensitive trace elements. For example, the Y/Ho ratios are greatest in shales proximal to mineralization and are generally lowest in the deeper footwall and upper hanging wall (Figs. 13–16). The Ce/Ce* values, however, are lowest near the mineralized horizon and become more positive toward the lower and upper parts of the stratigraphy (Figs. 13, 15). It is well established that fine-grained sediments deposited under varying redox conditions typically inherit the signatures of ambient seawater at the time of deposition (Elderfield and Greaves, 1981; Elderfield et al., 1988; de Baar et al., 1988, 1991; German et al., 1991; Goodfellow et al., 2003a; Edmonds and German, 2004). Whereas Y/Ho ratios of seawater probably have not drastically changed during Earth evolution and are generally redox independent (e.g., Bau and Dulski, 1996; Planavsky et al., 2010), the marine REE cycle, particularly Ce systematics, is strongly controlled by ocean redox (e.g., Elderfield et al., 1988; de Baar et al., 1988, 1991). Under oxidizing conditions, seawater and authigenic sediments have a pronounced negative Ce anomaly, due to the adsorption and incorporation of Ce into Mn oxides and Mn nodules that form under oxic ocean conditions (Elderfield et al., 1988). By contrast, in the case of a redox-chemocline, Mn oxides that formed in the oxic upper water column destabilize at depth and release excess Ce scavenged from the oxygenated water column, resulting in positive Ce anomalies within pelagic sediments (de Baar et al., 1988, 1991; Elderfield et al., 1988; Alibo and Nozaki, 1999). The REY systematics of Wolverine area samples least affected by alteration and mineralization, including the lowermost footwall samples from the Fisher zone and samples from the uppermost hanging wall, have remarkably similar REY signatures, with flat PAAS-normalized patterns and no to very small negative Ce anomalies (Ce/Ce* ~1), consistent with deposition under anoxic to suboxic conditions (Figs. 13–15). However, samples from the footwall and immediate hanging wall of the Wolverine deposit display more negative

Ce anomalies and much higher Y/Ho ratios (see Elderfield et al., 1988; de Baar et al., 1991; Bau, 1996; Nozaki et al., 1997; Alibo and Nozaki, 1999; Bau and Dulski, 1999). This finding is somewhat unexpected, given that those shales proximal to the Wolverine mineralized horizon display the greatest enrichments in redox-sensitive trace elements indicative of deposition under periodic euxinic conditions. There are potential solutions to this paradox, however, involving apatite and carbonate abundance (Fig. 19).

The inverse relationship between the Ce/Ce* anomalies and P_2O_5 concentrations observed in Figure 15b have been observed in other shale-rich sequences and have been interpreted to reflect detrital apatite in shales (Piper, 2001; Slack et al., 2004, 2015). The negative Ce/Ce* anomalies could be, in part, explained by apatite having formed in the shallower, oxygenated parts of the Wolverine basin where it inherited the signature of oxygenated surface waters, followed by deposition as detrital grains into deeper, less oxygenated waters. The relationship of Y/Ho to P_2O_5 also shows a weak positive correlation (Fig. 19a), suggesting that detrital apatite exerts some control on the Y/Ho ratios in the shales; however, there are also numerous higher values with lower P_2O_5 contents that cannot be solely explained by apatite detritus. In particular, Y/Ho and Ce/Ce* values show strong correlations with CO_2 contents in the shales (Fig. 19), implying that the ratios are also affected by carbonate content. The elevated Y/Ho ratios in many samples are very similar to, and trend toward, the value for modern seawater, thus implying that the carbonate present in the shales may have had a seawater origin (Fig. 15). A potential explanation for this trend is that the high Y/Ho ratios and low Ce/Ce* values were associated with enhanced carbonate precipitation from overlying oxygenated seawater above a lower euxinic zone (i.e., stratified basin). An alternative mechanism, and a more likely one based on geological and geochemical relationships, is that these ratios and values reflect a late hydrothermal overprint by low-temperature, CO_2-rich fluids that originated from oxygenated seawater, potentially as the basin was opening (Fig. 18). Although the Wolverine basin was restricted with partially euxinic conditions in lower bottom waters, it is possible that upper waters were oxygenated, and when drawn into the hydrothermal system these fluids overprinted the existing shales with carbonate alteration that had signatures similar to oxygenated seawater (Fig. 18). This interpretation is supported by the geology and alteration of the Wolverine deposit. For example, carbonate exhalative rocks exist both at the hanging-wall/footwall interface, and within the hanging-wall strata of the deposit (Fig. 5; Bradshaw et al., 2008). These carbonate exhalites are spatially associated with iron formations indicative of venting at low temperature (T <250°C; Peter, 2003). Furthermore, there is abundant footwall and hanging-wall carbonate alteration in the deposit (Peter et al., 2007; Bradshaw et al., 2008). These features are consistent with late overprinting by low-temperature, oxygenated and CO_2-rich seawater-derived hydrothermal fluids (Fig. 18).

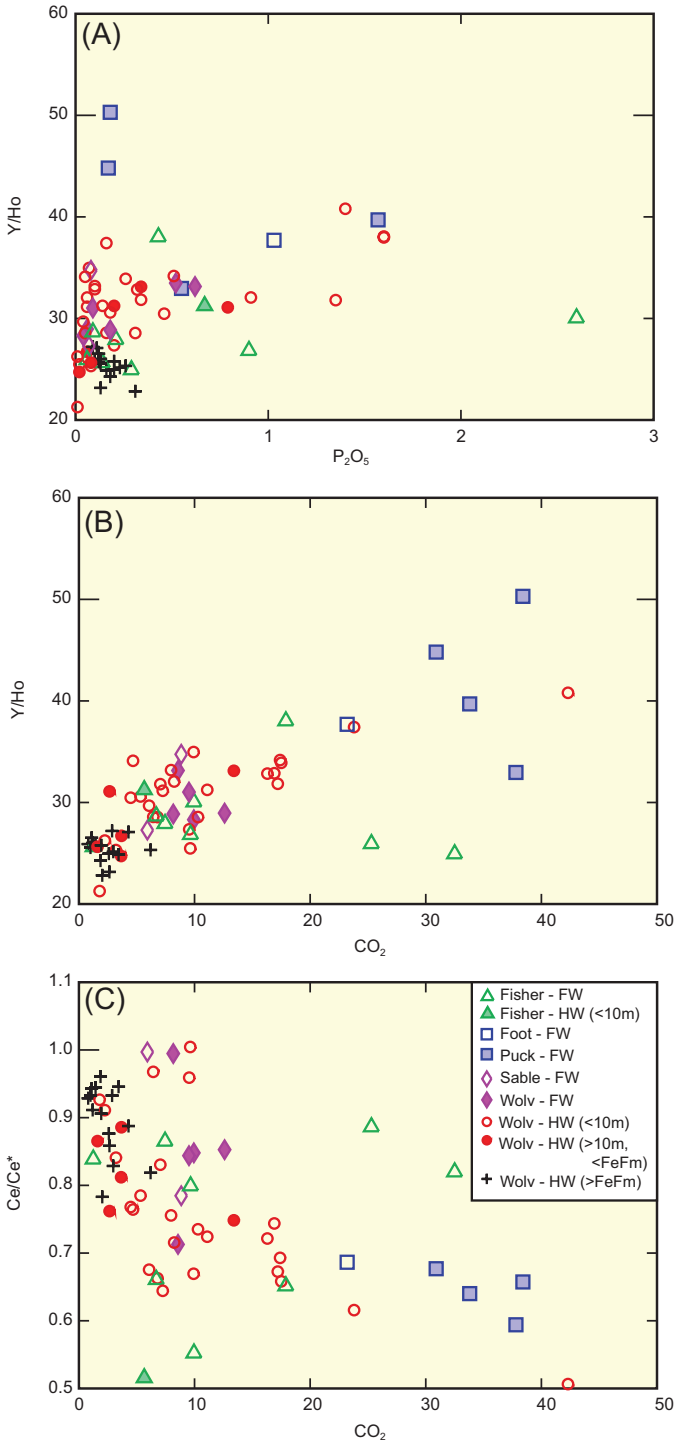

Fig. 19. (A). Y/Ho vs. P_2O_5 concentrations, (B), Y/Ho, and (C) Ce/Ce* vs. CO_2 concentrations. These results suggest that the REY systematics are strongly influenced by apatite abundance and carbonate content of the samples.

Shale geochemistry as an exploration vector

The shale lithofacies in the Wolverine deposit has numerous geochemical characteristics that provide insights into the ambient environment of formation, proportions of hydrothermal versus detrital components, and hydrothermal fluid-rock interaction. These data are useful as exploration vectors in shale-rich, siliciclastic felsic VMS environments; the results also have significance for sediment-hosted Zn-Pb environments. Whereas there is debate regarding the location of euxinia (i.e., bottom waters versus sediment column;

Gleeson et al., 2013; Reynolds et al., 2015), reduced sulfur at the site of deposition and euxinic conditions are important in the generation of some VMS deposits in sediment-rich environments, resulting in more efficient complexing of metals from hydrothermal vents (Goodfellow et al., 2003b). Identification of these conditions is best achieved using a multiproxy approach (Tribovillard et al., 2006; Lyons et al., 2009; Piper and Calvert, 2009; Little et al., 2015), and in the Wolverine deposit the combination of low Mn contents (<1,000 ppm); V-Cr-Ni systematics (i.e., high V/Cr and V/(V + Ni) ratios); U-Mo enrichment (i.e., U_{EF} and Mo_{EF} >10); and high S/$C_{organic}$ ratios (>0.32) and REY (Ce/Ce* ~1) systematics of unmineralized and relatively unaltered samples provide the best indicators of basin redox conditions. The REY systematics have also been useful in identifying late hydrothermal overprints and upwelling of lower temperature hydrothermal fluids. Those shales with late overprints are found proximal to the main mineralized horizon and have negative Ce anomalies (Ce/Ce* <1) and high Y/Ho ratios. However, it is uncertain if these REY systematics are unique to Wolverine or are applicable to all sediment-rich basins.

In addition to basin redox and vent proximity, major element and metal associations in shales can also provide vectors to mineralization. Shales that are spatially associated with mineralization typically have elevated contents of base metals, Fe-(Mn), and Fe-Mn-Ti-Al systematics typical of hydrothermal activity (Fig. 12). Furthermore, these shales exhibit well-developed metasomatic trends consistent with the effects of chlorite, sericite, and carbonate alteration, including high CIW values, with or without quartz alteration (Fig. 10).

Identifying shales with the combination of the right redox conditions of formation, evidence of hydrothermal vent proximity, and metal enrichment and alteration is a challenging task, but one that should allow target prioritization and reduced exploration risk.

Conclusions

Lithogeochemical data for shales from the Wolverine VMS deposit provide insight into ambient basinal conditions and the nature of hydrothermal activity during sulfide mineralization. Shales are located at various stratigraphic levels and occur in various mineralized zones within the Wolverine deposit area (e.g., Fisher, Puck, and Sable zones). Along the mineralized horizon near the immediate hanging wall and footwall, shales display evidence for deposition under anoxic conditions (e.g., low Mn, anoxic V-Cr-Mo-U systematics, S/$C_{organic}$ >0.32). In the deeper footwall and uppermost hanging wall, the shales have geochemical signatures that are indicative of suboxic to oxic conditions. The Mo-U systematics of the Wolverine shales suggest that the basin was euxinic during deposit formation with free H_2S present periodically in the water column, which contributed significantly to the sulfur budget of the deposit and was important in deposit genesis. Furthermore, the Mo-U systematics favor deposition in a restricted basin where H_2S formation via sulfate reduction was associated with excess organic carbon preservation (i.e., nutrient traps). There is also evidence of a progressive shift upward in the stratigraphy to more oxygenated conditions in strata of the uppermost hanging wall. The shift from euxinic to suboxic or oxic conditions is consistent with tectonic models that favor a change from rifting during Wolverine deposit formation, where the basin was restricted with minimal circulation, to development of a back-arc basin that was accompanied by extension and ingress of oxygenated seawater.

The Wolverine shales proximal to mineralization have elevated Y/Ho ratios and Ce/Ce* values <<1 indicative of oxygenated seawater. The Ce/Ce* values are associated with anomalous P_2O_5 contents and are interpreted to represent partial control by detrital apatite, where the negative Ce anomaly was inherited from oxygenated waters in the upper water column and then deposited to depth via a phosphate particulate shuttle. The Ce/Ce* and Y/Ho also correlate with CO_2, however, and shales having the strongest REY indicators similar to oxygenated seawater also display the strongest euxinic signatures. This paradoxical behavior can be reconciled by a late hydrothermal overprint on the shales from low-temperature, CO_2-rich (oxygenated) hydrothermal fluids (i.e., high Y/Ho but Ce/Ce* <<1), in a vent-proximal environment. This interpretation is consistent with data from geology, stratigraphy, and hydrothermal alteration in the immediate footwall and hanging wall of the Wolverine deposit.

The use of diagnostic geochemical parameters is useful for identifying shales in the Wolverine basin that are prospective for VMS mineralization and in similar basins globally. In particular, samples should display evidence for deposition under anoxic to euxinic conditions (i.e., Mn <1,000 ppm; high V-Mo-U and V/(V + Ni), U_{EF}, Mo_{EF}), hydrothermal Fe-Al-Mn signatures (i.e., high Fe/Al), and evidence for hydrothermal alteration (i.e., high CIW values, high molar sericite and chlorite). Identification of samples having these features is useful in targeting prospective VMS environments in shale-dominated successions and potential mineralized targets within shale-rich basins.

Acknowledgments

This research has been by funding from the Yukon Zinc Corporation, the NSERC Collaborative Research and Development program (Wolverine project), and NSERC Discovery Grants to Steve Piercey, Harold Gibson, and Balz Kamber. The research is also part of Canadian Mining Industry Research Organization (CAMIRO) Project 08E04 on the Geochemistry of Shales as Vectors to Ore Deposits funded by Actlabs, Barrick Gold Corporation, First Quantum Minerals Ltd., Hudbay Minerals Inc., Newmont Mining Corp., MMG Ltd., Selwyn Resources Ltd., Teck Corp., and Ur Energy Ltd., and an NSERC Collaborative Research and Development Grant (CRDPJ-387591-09). Steve Piercey is also supported by the NSERC-Altius Industrial Research Chair in Mineral Deposits funded by NSERC, Altius Resources Inc., and the Research and Development Corporation of Newfoundland and Labrador.

We are grateful for discussions with Geoff Bradshaw, Gilles Dessureau, Jason Dunning, Sarah Gleeson, Wayne Goodfellow, Graham Layne, Maribeth Moll, Dan Layton-Matthews, Don Murphy, and Jan Peter. These colleagues have shaped many of the views and arguments presented here, but any errors or omissions are the responsibility of the authors. Mary Devine is thanked for drafting some of the figures. Thomas Ulrich, Annette Gladu, and Claire Kamber provided help

and contributions during lab work at Laurentian University. We thank journal reviewers Nick Harris and Nicolas Tribovillard. *Economic Geology* editor John Slack is also thanked for thoughtful comments, editorial contributions, and answering numerous questions during the review process from the authors.

REFERENCES

Algeo, T.J., and Maynard, J.B., 2004, Trace-element behavior and redox facies in core shales of Upper Pennsylvanian Kansas-type cyclothems: Chemical Geology, v. 206, p. 289–318.

——2008, Trace-metal covariation as a guide to water-mass conditions in ancient anoxic marine environments: Geosphere, v. 4, p. 872–887.

Algeo, T.J., and Tribovillard, N., 2009, Environmental analysis of paleoceanographic systems based on molybdenum-uranium covariation: Chemical Geology, v. 268, p. 211–225.

Alibo, D.S., and Nozaki, Y., 1999, Rare earth elements in seawater: Particle association, shale-normalization, and Ce oxidation: Geochimica et Cosmochimica Acta, v. 63, p. 363–372.

Bau, M., 1996, Controls on the fractionation of isovalent trace elements in magmatic and aqueous systems: Evidence from Y/Ho, Zr/Hf, and lanthanide tetrad effect: Contributions to Mineralogy and Petrology, v. 123, p. 323–333.

Bau, M., and Dulski, P., 1996, Distribution of yttrium and rare-earth elements in the Penge and Kuruman iron-formations, Transvaal Supergroup, South Africa: Precambrian Research, v. 79, p. 37–55.

——1999, Comparing yttrium and rare earths in hydrothermal fluids from the Mid-Atlantic Ridge: Implications for Y and REE behaviour during near-vent mixing and for the Y/Ho ratio of Proterozoic seawater: Chemical Geology, v. 155, p. 77–90.

Berner, R.A., 1984, Sedimentary pyrite formation: An update: Geochimica et Cosmochimica Acta, v. 48, p. 605–615.

Berner, R.A., and Raiswell, R., 1983, Burial of organic carbon and pyrite sulfur in sediments over Phanerozoic time: A new theory: Geochimica et Cosmochimica Acta, v. 47, p. 855–862.

Boström, K., 1973, The origin and fate of ferromanganoan active ridge sediments: Stockholm Contributions to Geology, v. 27, p. 147–243.

Bradshaw, G., 2003, Geology and genesis of the Wolverine polymetallic volcanic rock-hosted massive sulphide (VHMS) deposit, Finlayson Lake district, Yukon, Canada: M.Sc.thesis, University of British Columbia, Vancouver, 172 p.

Bradshaw, G.D., Rowins, S.M., Peter, J.M., and Taylor, B.E., 2008, Genesis of the Wolverine volcanic sediment-hosted massive sulfide deposit, Finlayson Lake district, Yukon, Canada: Mineralogical, mineral chemical, fluid inclusion, and sulfur isotope evidence: Economic Geology, v. 103, p. 35–60.

Brauneder, K., Hamilton, S.M., and Hattori, K., 2016, Geochemical processes in the formation
of "forest rings:" Examples of reduced chimney formation in the absence of mineral deposits: Geochemistry: Exploration, Environment, Analysis, v. 16, p. 85–99.

Burnham, O.M., and Schweyer, J., 2004, Trace element analysis of geological samples by inductively coupled plasma mass spectrometry at the Geoscience Laboratories: Revised capabilities due to improvements to instrumentation: Ontario Geological Survey Summary of Fieldwork and Other Activities 2004, Open File 6145, p. 54.1–54.20.

Burnham, O.M., Hechler, J., Semenyna, L., and Schweyer, J., 2002, Mineralogical controls on the determination of trace elements following mixed-acid dissolution: Ontario Geological Survey Summary of Fieldwork and Other Activities 2002, Open File 6100, p. 36.1–36.12.

Calvert, S.E., and Pedersen, T.F., 1993, Geochemistry of Recent oxic and anoxic marine sediments: Implications for the geological record: Marine Geology, v. 113, p. 67–88.

——1996, Sedimentary geochemistry of manganese: Implications for the environment of formation of manganiferous black shales: Economic Geology, v. 91, p. 36–47.

Colpron, M., and Nelson, J.L., 2009, A Palaeozoic northwest passage: Incursion of Caledonian, Baltican and Siberian terranes into eastern Panthalassa, and the early evolution of the North American Cordillera: Geological Society of London Special Publication 318, p. 273–307.

Colpron, M., Nelson, J.L., and Murphy, D.C., 2006, A tectonostratigraphic framework for the pericratonic terranes of the northern Canadian Cordillera: Geological Association of Canada Special Paper 45, p. 1–23.

de Baar, H.J.W., German, C.R., Elderfield, H., and van Gaans, P., 1988, Rare earth element distributions in anoxic waters of the Cariaco trench: Geochimica et Cosmochimica Acta, v. 52, p. 1203–1219.

de Baar, H.J.W., Schijf, J., and Byrne, R.H., 1991, Solution chemistry of the rare earth elements in seawater: European Journal of Solid State Inorganic Chemistry, v. 28, p. 357–373.

Eastoe, C.J., and Gustin, M.M., 1996, Volcanogenic massive sulfide deposits and anoxia in the Phanerozoic oceans: Ore Geology Reviews, v. 10, p. 179–197.

Edmonds, H.N., and German, C.R., 2004, Particle geochemistry in the Rainbow hydrothermal plume, Mid-Atlantic Ridge: Geochimica et Cosmochimica Acta, v. 68, p. 759–772.

Elderfield, H., and Greaves, M.J., 1981, Negative cerium anomalies in the rare earth element patterns of oceanic ferromanganese nodules: Earth and Planetary Science Letters, v. 55, p. 163–170.

Elderfield, H., Charnock, H., Lovelock, J.E., Liss, P. S., and Whitfield, M., 1988, The oceanic chemistry of the rare-earth elements: Philosophical Transactions of the Royal Society of London, Series A: Mathematical and Physical Sciences, v. 325, p. 105–124.

Emerson, S.R., and Huested, S.S., 1991, Ocean anoxia and the concentrations of molybdenum and vanadium in seawater: Marine Chemistry, v. 34, p. 177–196.

Franklin, J.M., Gibson, H.L., Galley, A.G., and Jonasson, I.R., 2005, Volcanogenic massive sulfide deposits: Economic Geology 100th Anniversary Volume, p. 523–560.

Galley, A.G., Hannington, M., and Jonasson, I., 2007, Volcanogenic massive sulphide deposits: Geological Association of Canada, Mineral Deposits Division, Special Publication 5, p. 141–161.

German, C.R., Holliday, B.P., and Elderfield, H., 1991, Redox cycling of rare earth elements in the sub-oxic zone of the Black Sea: Geochimica et Cosmochimica Acta, v. 55, p. 3553–3558.

Gleeson, S.A., Paradis, S., Magnall, J., and Reynolds, M.A., 2013, Sedex deposits in the northern Cordillera: Where are we in the basin, and what role does water column euxinia really play? [abs.]: Society of Economic Geologists, Whistler 2013: Geoscience for Discovery, Whistler, BC, Canada, September 2013, Program with Abstracts, p. 20–21.

Goodfellow, W.D., 1987, Anoxic stratified oceans as a source of sulphur in sediment-hosted
stratiform Zn-Pb deposits (Selwyn Basin, Yukon, Canada): Chemical Geology, v. 65, p. 359–382.

Goodfellow, W.D., and Peter, J.M., 1996, Sulfur isotope composition of the Brunswick No.12 massive sulfide deposit, Bathurst mining camp, New Brunswick: Implications for ambient environment, sulfur source and ore genesis: Canadian Journal of Earth Sciences, v. 33, p. 231–251.

Goodfellow, W.D., McCutcheon, S.R., and Peter, J.M., 2003a, Massive sulfide deposits of the Bathurst mining camp, New Brunswick and northern Maine: Introduction and summary of findings: Economic Geology Monograph 11, p. 1–16.

Goodfellow, W.D., Peter, J.M., Winchester, J.A., and van Staal, C.R., 2003b, Ambient marine environment and sediment provenance during formation of massive sulfide deposits in the Bathurst mining camp: Importance of reduced bottom waters to sulfide precipitation and preservation: Economic Geology Monograph 11, p. 129–156.

Grant, S.L., 1997, Geochemical, radiogenic tracer isotopic, and U-Pb geochronological studies of Yukon-Tanana terrane rocks from the Money klippe, southeastern Yukon, Canada: M.Sc.thesis, Edmonton, Alberta, University of Alberta, 177 p.

Hatch, J.R., and Leventhal, J.S., 1992, Relationship between inferred redox potential of the depositional environment and geochemistry of the Upper Pennsylvanian (Missourian) Stark Shale Member of the Dennis Limestone, Wabaunsee County, Kansas, U.S.A: Chemical Geology, v. 99, p. 65–82.

Jones, B., and Manning, D.A.C., 1994, Comparison of geochemical indices used for the interpretation of palaeoredox conditions in ancient mudstones: Chemical Geology, v. 111, p. 111–129.

Kamber, B.S., 2009, Geochemical fingerprinting: 40 years of analytical development and real world applications: Applied Geochemistry, v. 24, p. 1074–1086.

Kamber, B.S., and Webb, G.E., 2001, The geochemistry of Late Archaean microbial carbonate: Implications for ocean chemistry and continental erosion history: Geochimica et Cosmochimica Acta, v. 65, p. 2509–2525.

Large, R.R., Allen, R.L., Blake, M.D., and Herrmann, W., 2001, Hydrothermal alteration and volatile element halos for the Rosebery K Lens volcanic-hosted massive sulfide deposit, western Tasmania: Economic Geology, v. 96, p. 1055–1072.

Leventhal, J.S., 1983, An interpretation of carbon and sulfur relationships in Black Sea sediments as indicators of environments of deposition: Geochimica et Cosmochimica Acta, v. 47, p. 133–137.
Little, S.H., Vance, D., Lyons, T.W., and McManus, J., 2015, Controls on trace metal authigenic enrichment in reducing sediments: Insights from modern oxygen-deficient settings: American Journal of Science, v. 315, p. 77–119.
Lyons, T.W., Anbar, A.D., Severmann, S., Scott, C., and Gill, B.C., 2009, Tracking euxinia in the ancient ocean: A multiproxy perspective and Proterozoic case study: Annual Review of Earth and Planetary Sciences, v. 37, p. 19–48.
Marx, S.K., and Kamber, B.S., 2010, Trace-element systematics of sediments in the Murray-Darling Basin, Australia: Sediment provenance and palaeoclimate implications of fine scale chemical heterogeneity: Applied Geochemistry, v. 25, p. 1221–1237.
McLennan, S.M., 1989, Rare earth elements in sedimentary rocks: Influence of provenance and sedimentary processes: Reviews in Mineralogy, v. 21, p. 169–200.
McLennan, S.M., Taylor, S.R., McCulloch, M.T., and Maynard, J.B., 1990, Geochemical and Nd-Sr isotopic composition of deep-sea turbidites: Crustal evolution and plate tectonic associations: Geochimica et Cosmochimica Acta, v. 54, p. 2015–2050.
Menor-Salvan, C., Tornos, F., Fernandez-Remolar, D., and Amils, R., 2010, Association between catastrophic paleovegetation changes during Devonian-Carboniferous boundary and the formation of giant massive sulfide deposits: Earth and Planetary Science Letters, v. 299, p. 398–408.
Meyer, K.M., and Kump, L.R., 2008, Oceanic euxinia in Earth history: Causes and consequences: Annual Review of Earth and Planetary Sciences, v. 36, p. 251–288.
Mortensen, J.K., 1992, Pre-Mid-Mesozoic tectonic evolution of the Yukon-Tanana terrane, Yukon and Alaska: Tectonics, v. 11, p. 836–853.
Murphy, D.C., Mortensen, J.K., Piercey, S.J., Orchard, M.J., and Gehrels, G.E., 2006, Tectonostratigraphic evolution of Yukon-Tanana terrane, Finlayson Lake massive sulphide district, southeastern Yukon: Geological Association of Canada Special Paper 45, p. 75–105.
Nelson, J.L., Colpron, M., and Israel, S., 2013, The Cordillera of British Columbia, Yukon, and Alaska: Tectonics and metallogeny: Society of Economic Geologists Special Publication 17, p. 53–109.
Nelson, J.L., Colpron, M., Piercey, S.J., Murphy, D.C., Dusel-Bacon, C., and Roots, C.F., 2006, Paleozoic tectonic and metallogenetic evolution of pericratonic terranes in Yukon, northern British Columbia and eastern Alaska: Geological Association of Canada Special Paper 45, p. 323–360.
Nesbitt, H.W., 2003, Petrogenesis of siliciclastic sediments and sedimentary rocks: Geological Association of Canada, GEOText 4, p. 39–52.
Nesbitt, H.W., and Young, G.M., 1984, Prediction of some weathering trends of plutonic and volcanic rocks based on thermodynamic and kinetic considerations: Geochimica et Cosmochimica Acta, v. 48, p. 1523–1534.
Nozaki, Y., Zhang, J., and Amakawa, H., 1997, The fractionation between Y and Ho in the marine environment: Earth and Planetary Science Letters, v. 148, p. 329–340.
Ohmoto, H., 1996, Formation of volcanogenic massive sulfide deposits: The Kuroko perspective: Ore Geology Reviews, v. 10, p. 135–177.
Pearson, C., and Giroux, G.A., 2006, Wolverine mineral property resource estimation: National Instrument 43-101 Independent Technical Report for Yukon Zinc Corporation: Toronto, 118 p.
Peter, J.M., 2003, Ancient iron formations: Their genesis and use in the exploration for stratiform base metal sulphide deposits, with examples from the Bathurst mining camp: Geological Association of Canada, GEOText 4, p. 145–176.
Peter, J.M., Layton-Matthews, D., Piercey, S., Bradshaw, G., Paradis, S., and Boulton, A., 2007, Volcanic-hosted massive sulphide deposits of the Finlayson Lake district, Yukon: Geological Association of Canada, Mineral Deposits Division, Special Publication 5, p. 471–508.
Piercey, S.J., Murphy, D.C., Mortensen, J.K., and Paradis, S., 2001a, Boninitic magmatism in a continental margin setting, Yukon-Tanana terrane, southeastern Yukon, Canada: Geology, v. 29, p. 731–734.
Piercey, S.J., Paradis, S., Murphy, D.C., and Mortensen, J.K., 2001b, Geochemistry and paleotectonic setting of felsic volcanic rocks in the Finlayson Lake volcanic-hosted massive sulfide district, Yukon, Canada: Economic Geology, v. 96, p. 1877–1905.
Piercey, S.J., Paradis, S., Peter, J.M., and Tucker, T.L., 2002, Geochemistry of basalt from the Wolverine volcanic-hosted massive-sulphide deposit, Finlayson Lake district, Yukon Territory: Geological Survey of Canada, Current Research 2002-A3, 11 p.
Piercey, S.J., Mortensen, J.K., and Creaser, R.A., 2003, Neodymium isotope geochemistry of felsic volcanic and intrusive rocks from the Yukon-Tanana terrane in the Finlayson Lake region, Yukon, Canada: Canadian Journal of Earth Sciences, v. 40, p. 77–97.
Piercey, S.J., Murphy, D.C., Mortensen, J.K., and Creaser, R.A., 2004, Mid-Paleozoic initiation of the northern Cordilleran marginal back-arc basin: Geological, geochemical and neodymium isotopic evidence from the oldest mafic magmatic rocks in Yukon-Tanana terrane, Finlayson Lake district, southeast Yukon, Canada: Geological Society of America Bulletin, v. 116, p. 1087–1106.
Piercey, S.J., Nelson, J.L., Colpron, M., Dusel-Bacon, C., Simard, R.-L., and Roots, C.F., 2006, Paleozoic magmatism and crustal recycling along the ancient Pacific margin of North America, northern Cordillera: Geological Association of Canada Special Paper 45, p. 281–322.
Piercey, S.J., Peter, J.M., Mortensen, J.K., Paradis, S., Murphy, D.C., and Tucker, T.L., 2008, Petrology and U-Pb geochronology of footwall porphyritic rhyolites from the Wolverine volcanogenic massive sulfide deposit, Yukon, Canada: Implications for the genesis of massive sulfide deposits in continental margin environments: Economic Geology, v. 103, p. 5–33.
Piercey, S.J., Murphy, D.C., and Creaser, R.A., 2012, Lithosphere-asthenosphere mixing in a transform-dominated late Paleozoic backarc basin: Implications for northern Cordilleran crustal growth and assembly: Geosphere, v. 8, p. 716–739.
Piper, D.Z., 1994, Seawater as the source of minor elements in black shales, phosphorites and other sedimentary rocks: Chemical Geology, v. 114, p. 95–114.
——2001, Marine chemistry of the Permian Phosphoria Formation and basin, southeast Idaho: Economic Geology, v. 96, p. 599–620.
Piper, D.Z., and Calvert, S.E., 2009, A marine biogeochemical perspective on black shale deposition: Earth-Science Reviews, v. 95, p. 63–96.
Planavsky, N., Bekker, A., Rouxel, O.J., Kamber, B., Hofmann, A., Knudsen, A., and Lyons, T.W., 2010, Rare earth element and yttrium compositions of Archean and Paleoproterozoic Fe formations revisited: New perspectives on the significance and mechanisms of deposition: Geochimica et Cosmochimica Acta, v. 74, p. 6387–6405.
Plint, H.E., and Gordon, T.M., 1997, The Slide Mountain terrane and the structural evolution of the Finlayson Lake fault zone, southeastern Yukon: Canadian Journal of Earth Sciences, v. 34, p. 105–126.
Quinby-Hunt, M.S., and Wilde, P., 1994, Thermodynamic zonation in the black shale facies based on iron-manganese-vanadium content: Chemical Geology, v. 113, p. 297–317.
——1996, Chemical depositional environments of calcic marine black shales: Economic Geology, v. 91, p. 4–13.
Raiswell, R., and Berner, R.A., 1985, Pyrite formation in euxinic and semi-euxinic sediments: American Journal of Science, v. 285, p. 710–724.
Reynolds, M.A., Gingras, M.K., Gleeson, S.A., and Stemler, J.U., 2015, More than a trace of oxygen: Ichnological constraints on the formation of the giant Zn-Pb-Ag ± Ba deposits, Red Dog district, Alaska: Geology, v. 43, p. 867–870.
Sáez, R., Moreno, C., González, F., and Almodóvar, G., 2011, Black shales and massive sulfide deposits: Causal or casual relationships? Insights from Rammelsberg, Tharsis, and Draa Sfar: Mineralium Deposita, v. 46, p. 585–614.
Scott, C., and Lyons, T.W., 2012, Contrasting molybdenum cycling and isotopic properties in euxinic versus non-euxinic sediments and sedimentary rocks: Refining the paleoproxies: Chemical Geology, v. 324–325, p. 19–27.
Slack, J.F., Dumoulin, J.A., Schmidt, J.M., Young, L.E., and Rombach, C.S., 2004, Paleozoic sedimentary rocks in the Red Dog Zn-Pb-Ag district and vicinity, western Brooks Range, Alaska: Provenance, deposition, and metallogenic significance: Economic Geology, v. 99, p. 1385–1414.
Tornos, F., Solomon, M., Conde, C., and Spiro, B.F., 2008, Formation of the Tharsis massive sulfide deposit, Iberian pyrite belt: Geological, lithogeochemical, and stable isotope evidence for deposition in a brine pool: Economic Geology, v. 103, p. 185–214.
Tribovillard, N., Algeo, T.J., Lyons, T., and Riboulleau, A., 2006, Trace metals as paleoredox and paleoproductivity proxies: An update: Chemical Geology, v. 232, p. 12–32.